CHAPTER 5

MEASUREMENTS OF HELIUM METASTABLE DENSITY DECAY

5.1 INTRODUCTION

In Chapter 4, the conclusion that Penning collisions alone are responsible for populating the $5s^2\ ^2D_{5/2}$ level of Cd II late in the afterglow was based on the observation of an exponential decay of the 4416 Å emission at these times as well as careful evaluation of those changes produced on (the nature of) the exponential decay by variations of the cadmium concentration and helium pressure. To provide a firmer basis for this conclusion it is essential that the decay of the He (2^3S) metastable species be measured and compared with the corresponding decay of the 4416 Å spontaneous emission.

Before proceeding with a discussion of the experimental technique, section 5.2.1 outlines the theory by which the temporal evolution of the He (2^3S) and He (2^1S) densities were made in the afterglow. The method adopted utilized the Ladenburg-Reiche line absorption technique and in particular the time dependence of the line absorption.

The experimental method is described in section 5.2.2. For these experiments, light from two separate discharge segments was observed as the current (voltage) to one segment, that nearest the detectors, was terminated so as to create a stationary afterglow. The temporal evolution of the intensity regrowth signals at 3889 Å and 5016 Å was used to determine the decay of the triplet and singlet metastable species respectively.

To improve the quality of the experimental data, the same digitizing equipment and data processing software, as used in the investigation of the 4416 Å decay, was utilized in this present study. A number of experimental difficulties had to be overcome and these are discussed in section 5.2.3. The major difficulties were associated with establishing a compromise between the magnitude of the detector output signal and the response time of the detection equipment and also that of the observation of an apparent shift in the zero intensity signal due to the presence of a small d.c. offset in the detection equipment.

Results of the study of the He (2^3S) decay as a function of the cadmium neutral density are presented and discussed in section 5.4.1. Due to the weak signals at 3889 Å, the resulting relatively poor signal to noise ratio meant that no significant variation in the decay rate of the He (2^3S) density was observed for variations in either the helium pressure or discharge current.

As a function of the cadmium concentration, the He(2^3S) density was found to decay exponentially in the afterglow and to correlate well (section 5.4.2) with the corresponding late afterglow decay of the 4416 Å emission thus providing conclusive evidence that Penning collisions dominate the upper level production at these times. The experimental results did not, however, correlate quantitatively with the theoretical calculations, a result attributed to experimental problems associated with the heating of the oven sidearm used to supply the cadmium vapour.

In section 4.5.3 the results of measurements of the decay of the He (2^1S) density are presented. The decay of the singlet metastable species was found to be much more rapid than that of the triplet species, a result explained by singlet to triplet metastable conversion via

collisions of the second kind. This result was particularly significant as it alluded to the role of the numerous slow thermal electrons in depopulating higher lying states of helium in the early afterglow.

5.2 THEORY AND EXPERIMENTAL METHOD

5.2.1 Theory

The decay of excited state species in the hollow cathode discharge can be easily determined using the Ladenburg-Reiche line absorption method. In this, the measured parameter is the line absorption A_L, which is given by

$$A_L = 1 - \frac{\text{Transmitted Intensity}}{\text{Incident Intensity}} \qquad (5.1)$$

In this section an expression for the line absorption will be derived in order that the experimentally determined value of A_L can be related to the density of absorbing species.

The light intensity per unit frequency range for a simple Doppler broadened line, received at the spectrometer from a discharge segment of length 1 is (section 2.3.1)

$$I(\nu)_{em} = \frac{I_0}{k_0} \left[1 - \exp\left(-k_0 l e^{-\omega^2}\right)\right] d\nu \qquad (5.2)$$

Equation 5.2 represents the radiation incident upon the spectrometer in the absence of any absorption in the region between the emitting plasma and the detector.

If an absorbing medium of length l' and absorption coefficient k'_ν is

placed between the emitter and spectrometer then the total light intensity/unit frequency reaching the detectors is

$$I(\nu)_{Trans} = I(\nu)_{em} \exp(-k'_{\nu} l')$$

Integrating over frequency gives the total light intensity collected from the emitter after passing through the absorber as

$$I(\nu)_{Trans} = \frac{I_0}{k_0} \int_{-\infty}^{\infty} [1 - \exp(-k_0 l e^{-\omega^2})] \exp(-k'_{\nu} l') \, d\nu \quad (5.3)$$

If we consider the absorption line to be a simple Doppler broadened profile then

$$k'_{\nu} = k'_0 \, e^{-\omega'^2}$$

where k'_0 is the maximum absorption coefficient and ω' is given by

$$\omega' = \frac{2(\nu - \nu_0)(\ln 2)^{\frac{1}{2}}}{\Delta\nu'_D}$$

and $\Delta\nu'_D$ is the Doppler width of the absorption line.

Hence we arrive at an expression for the absorption A_L as

$$A_L = \frac{\int_{-\infty}^{\infty} [1 - \exp(-k_0 l \, e^{-\omega^2})] \, [1 - \exp(-k'_0 l' e^{-\omega'^2})] \, d\nu}{\int_{-\infty}^{\infty} [1 - \exp(-k_0 l \, e^{-\omega^2})] \, d\nu} \quad (5.4)$$

In the calculation of A_L from equation (5.4) two simplifications can be made. Studies in the helium afterglow by Deloche et al. (1976) have indicated that the gas temperature remains constant independent of time during the first 2 msec of the afterglow. This time is much longer than the volume destruction processes occurring in the discharge (typically $<<$ 100 μsec) and, for the duration of the afterglow studied in the

experiment we can write

$$\left[T_g \right]_{emitter} = \left[T_g \right]_{absorber}$$

which gives

$$\Delta\nu_D = \Delta\nu'_D$$

and hence

$$\omega = \omega'$$

If this assumption is not valid and the gas temperature relaxes from its value under steady state operation to its minimum value corresponding to the tube wall temperature (in this case 620 K) the size of the error incurred by this is always less than 10% over the entire range of absorption coefficients considered.

Finally, provided that the diffusion time of the absorbing species is small compared with other destruction mechanisms in the afterglow then

$$l' = l$$

and equation 5.4 can be re-written as

$$A_L = \frac{\int_{-\infty}^{\infty} \left[1 - \exp\left(-k_0 l\, e^{-\omega^2}\right)\right]\left[1 - \exp\left(-k'_0 l\, e^{-\omega^2}\right)\right] d\nu}{\int_{-\infty}^{\infty} \left[1 - \exp\left(-k_0 l\, e^{-\omega^2}\right)\right] d\nu} \qquad (5.5)$$

Equation 5.5 applies only to a simple Doppler broadened line. To extend the analysis to include complex lines with overlapping Doppler broadened components the procedure presented in section 2.3.3 applies.

Using equation 5.5 tables of $k'_o l$ versus absorption A_L were constructed for particular values of $k_o l$ of the emitter, values of which

had been previously determined by the d.c. fractional absorption method. The calculation was performed using a computer based numerical integration procedure and typical results of these calculations are shown in Figures 5.1 and 5.2. By measuring the absorption A_L at different times in the afterglow the corresponding value of $k'_o l$ may be determined. These $k'_o l$ values are related to the number density (or reduced number density) of the absorbing species by the relationship given in equation (2.6).

5.2.2 Experimental Method

A schematic diagram of the experimental apparatus is shown in Figure 5.3. The light intensity, from two disharge segments with non-overlapping glow regions, was analysed with the optical system, spectrometer and data acquisition system described in Chapter 4.

For the purposes of the discussion we will designate the discharge region nearest the detector as the absorber and the other discharge segment the emitter. As the emitter and absorber have identical discharge geometries and are operated under identical conditions the analysis of the experiment is identical to that described in section 5.2.1.

To determine the metastable density in the hollow cathode afterglow the variation in the intensity of the light from the emitter is recorded after the current in the absorber has been rapidly terminated in the manner described for the spontaneous emission studies of Chapter 4. Immediately following the termination of the discharge current, the number density of absorbing atoms is high, resulting in a large degree of

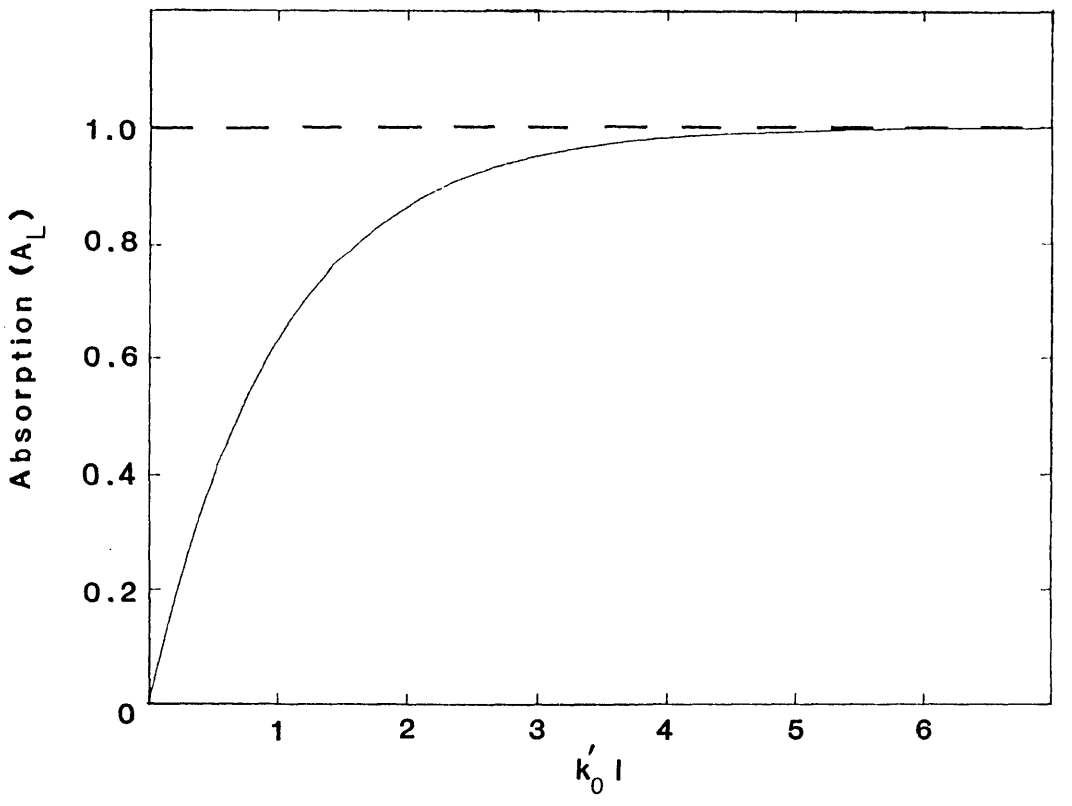

Figure 5.1 5016 Å Absorption (A_L) versus $k_0' l$ for a $k_0 l$ value of the emitter of 1.79

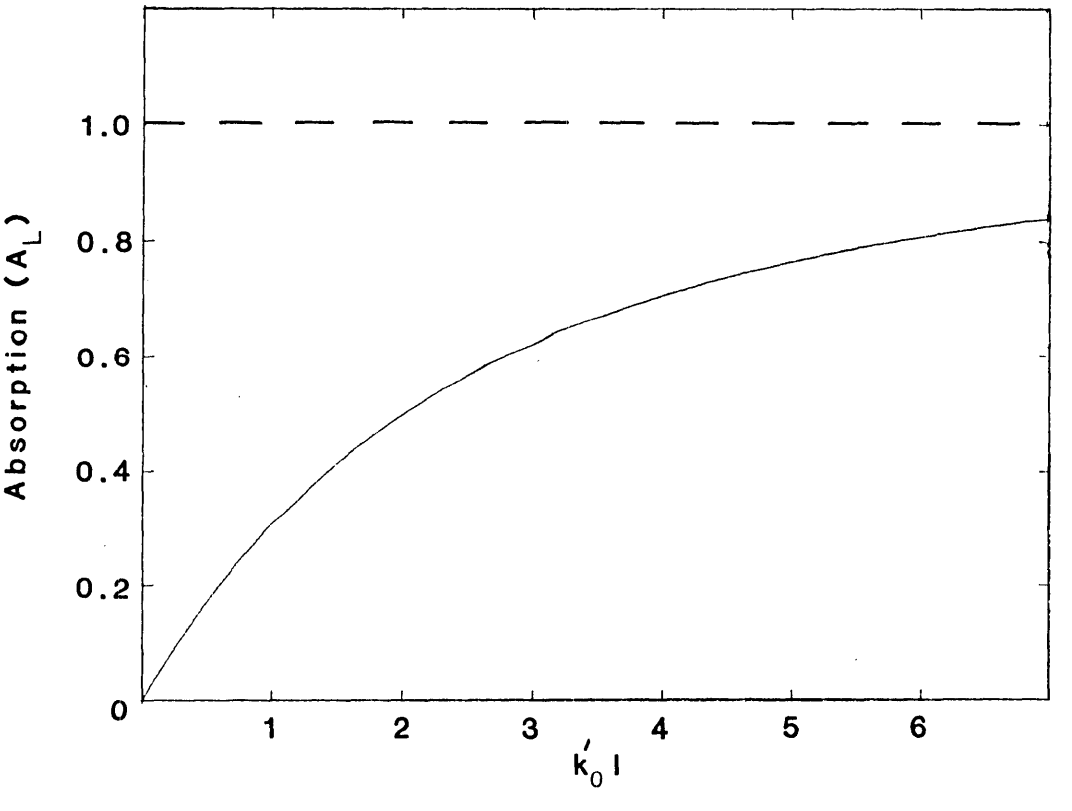

Figure 5.2 3889 Å Absorption (A_L) versus $k_0' l$ for a $k_0 l$ value of the emitter of 7.2

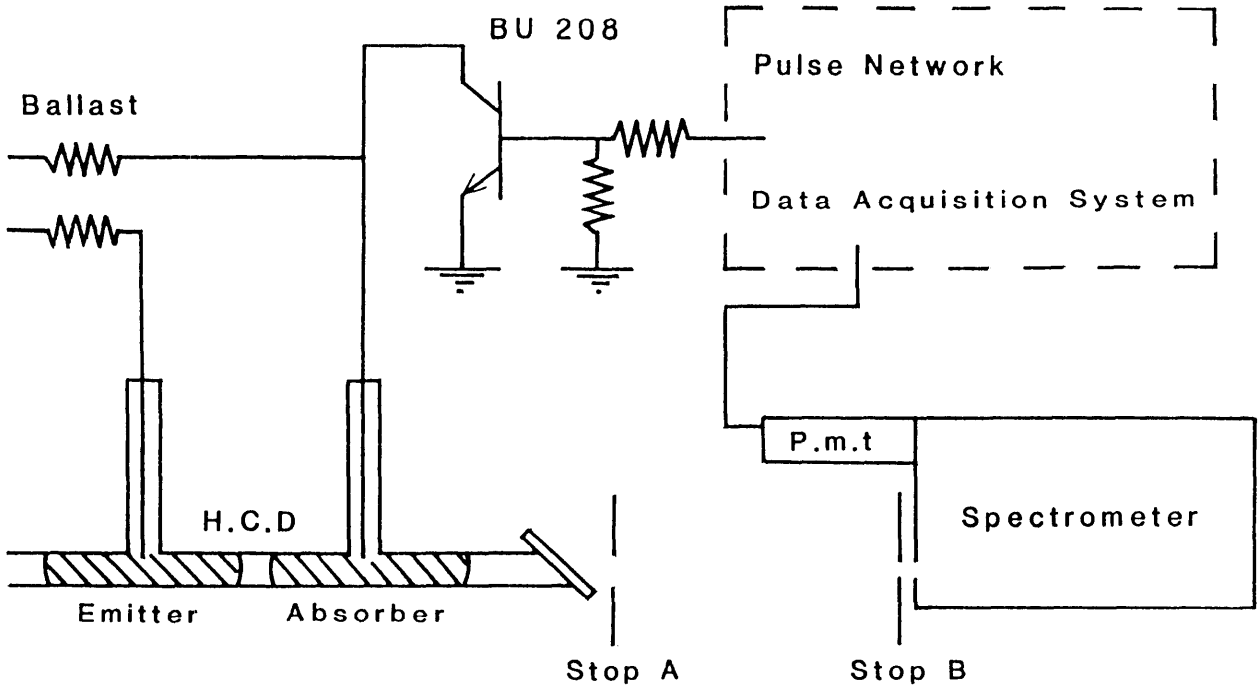

Figure 5.3 Schematic diagram of the experimental arrangement used in the measurement of the decay of excited species in the afterglow

absorption of light from the emitter. As the density of the absorbing species decays, through various collision processes and diffusion, the degree of absorption decreases and more light from the emitter reaches the detector. Late in the afterglow when absorption is minimal, the observed intensity is the total radiation from the emitter incident on the absorbing region.

A typical output, showing the intensity variation of the He I 3889 Å transition (terminating on the 2^3S level) is shown in Figure 5.4. As in Chapter 4, the point labelled T=0 represents the channel number at which the afterglow is created and the signal to the left of this point is that

due to the intensity at 3889 Å from two discharge segments.

From the intensity regrowth curve (Figure 5.4) the line absorption A_L can be calculated from a measurement of the transmitted intensity ($I_T(t)$), the incident intensity (I_E) and equation (5.1). Since I_T is a function of time in the afterglow the method detailed in section 5.2.1 allows the temporal dependence of the line absorption to be related to that of number density of the absorbing species.

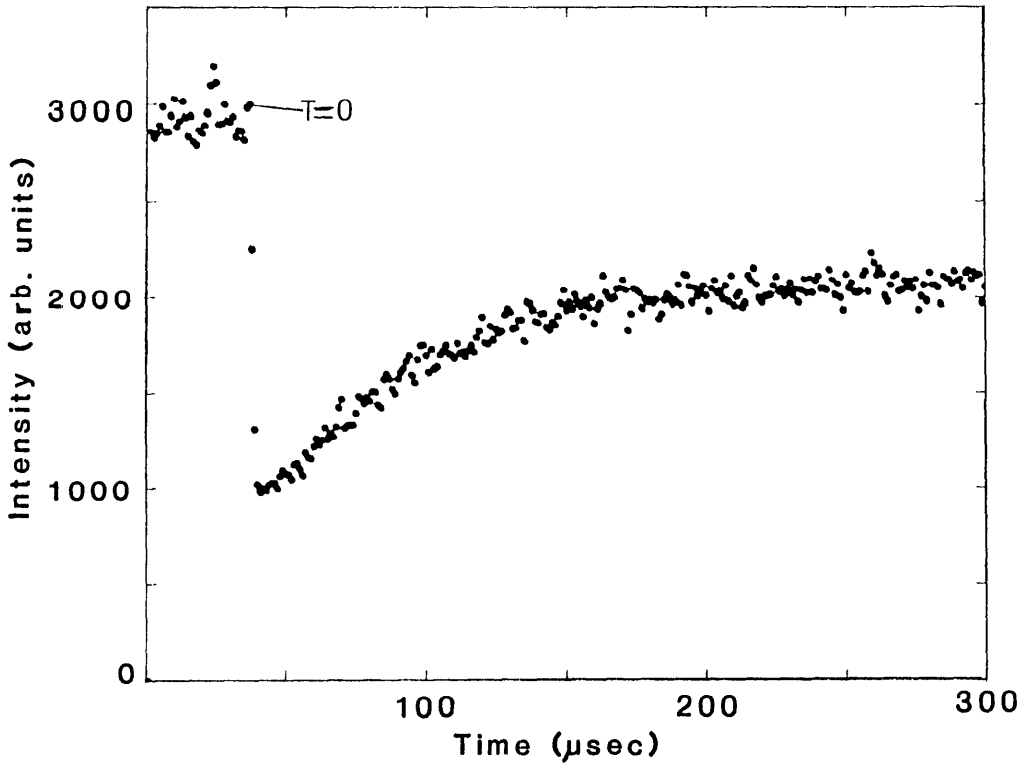

Figure 5.4 Typical result showing the 3889 Å intensity variation from the emitter for discharge conditions of 225^{0}C oven temperature, 20 Torr helium pressure and a current of 120 mA/anode. Each data point represents a time interval of 1 μsec

5.2.3 Experimental Difficulties

Because of the low intensity at 3889 Å, to develop signals of sufficient clarity for an accurate measurement of the line absorption, the output resistance of the photomultiplier was increased from the value of 3.3kΩ, used in the spontaneous emission studies of Chapter 4, to 22kΩ thereby increasing the system response to ~3 μsec. Thus the price paid for increased signal is a loss of temporal resolution in the early afterglow where the more rapid changes of the signal received at the detector may occur. However, at present we are concerned with the decay mechanisms late in the afterglow and this loss of temporal resolution can be tolerated if it results in an improved signal to noise ratio.

An additional complication came from the fact that the output of the AM 502 amplifier, used to amplify the photomultiplier signal, was found to have a small d.c. bias giving rise to an apparent shift in the zero intensity signal. The procedure used to eliminate this effect was to follow each accumulation of the intensity regrowth signal by the accumulation, for the same number of repetitions of the afterglow, of the signal with the spectrometer slits covered. This signal was subtracted from that stored in memory and the resulting waveform consisted only of the intensity of the transition studied with no component due to the amplifier offset.

5.3 INFLUENCE OF THE UPPER LEVEL POPULATIONS

As discussed in section 2.3.2, absorption experiments will only give the absolute number density of the absorbing species (N_1) provided the

condition $g_1 N_u << g_u N_1$ is satisfied. It is necessary to examine the afterglow to ensure that this condition holds at all times. If this condition is not valid then only the reduced number density can be determined.

Because it was not possible to measure directly the influence of the upper level population on the absorption at 3889 Å, the following argument was developed. When operated under d.c. conditions the effects of the upper level populations on the absorption coefficient (k_o) have been found to be minimal (Chapter 3). In the afterglow it is expected that the population densities of the high lying He I levels (>2^3S, 2^1S) will relax quickly via radiative decay and electronic de-excitation processes. This is supported by the observation that the 3889 Å spontaneous emission, or in fact any He I transition, decays to zero in times ~1 μsec in the afterglow (c.f. diagram 4.4). Thus it is expected that upper level effects will be much less significant than in the d.c. discharge and hence will not influence the calculation of the absolute density of the absorbing species from the measurement of the line absorption.

5.4 RESULTS

5.4.1 Variation with Oven Temperature of the Decay of the 2^3S Density

Following signal averaging over 300 separate afterglow events, results of the experiment showing the regrowth of the He I 3889 Å intensity as a function of oven temperature, for discharge conditions of 120 mA/anode and 20 Torr helium, are shown in Figures 5.5a - 5.7a. No

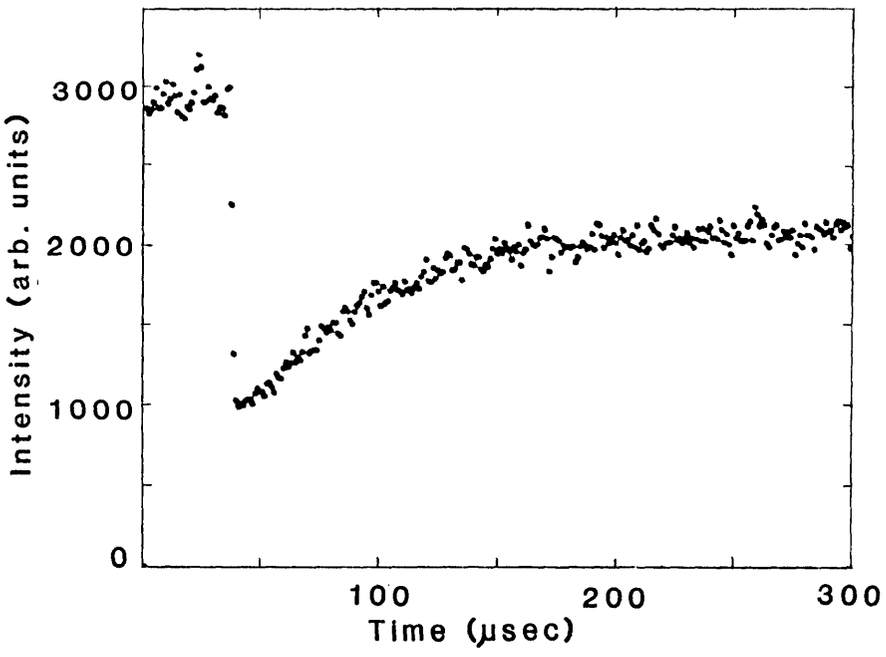

Figure 5.5a *3889 Å intensity regrowth curve for discharge conditions of 225°C oven temperature, 20 Torr helium and 120 mA/anode discharge current. (Each data point represents 1 μsec)*

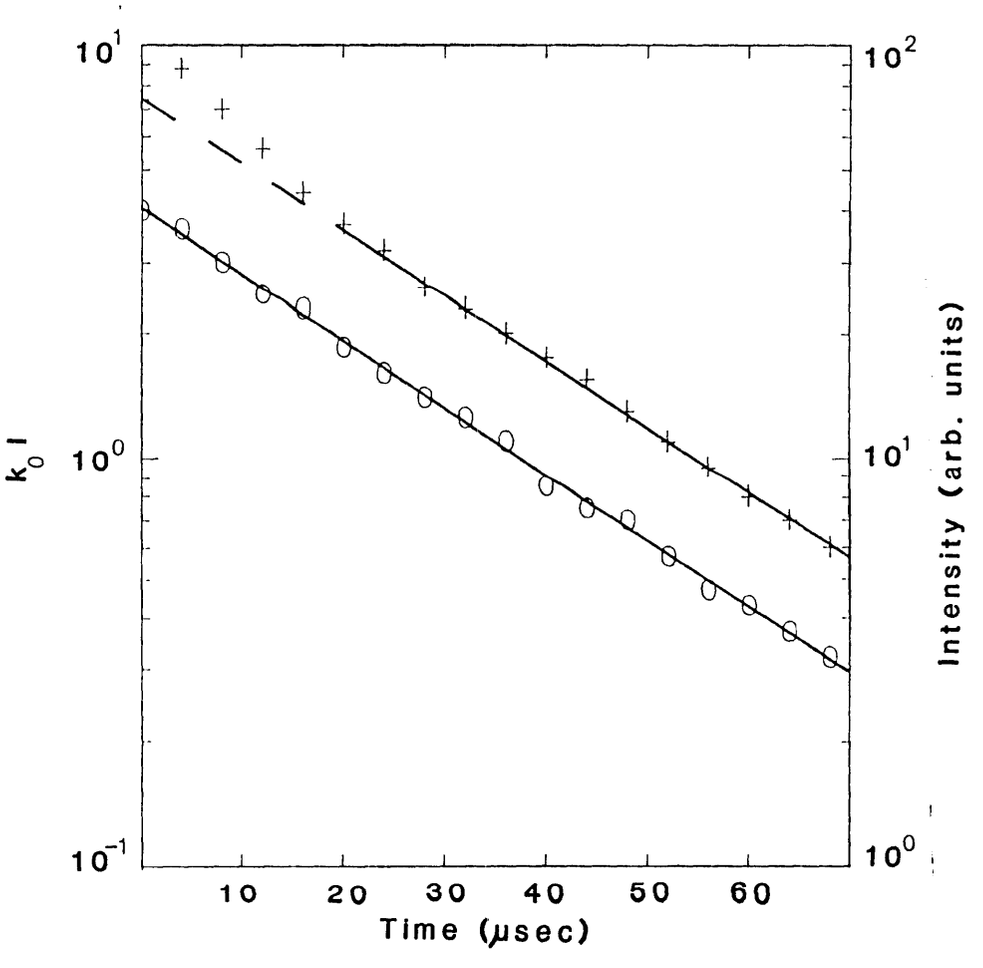

Figure 5.5b *Semi-logarithmic plots of the 4416 Å intensity (+) and the 2^3S metastable density (0) as a function of time after current termination. Discharge conditions as for Figure 5.5a*

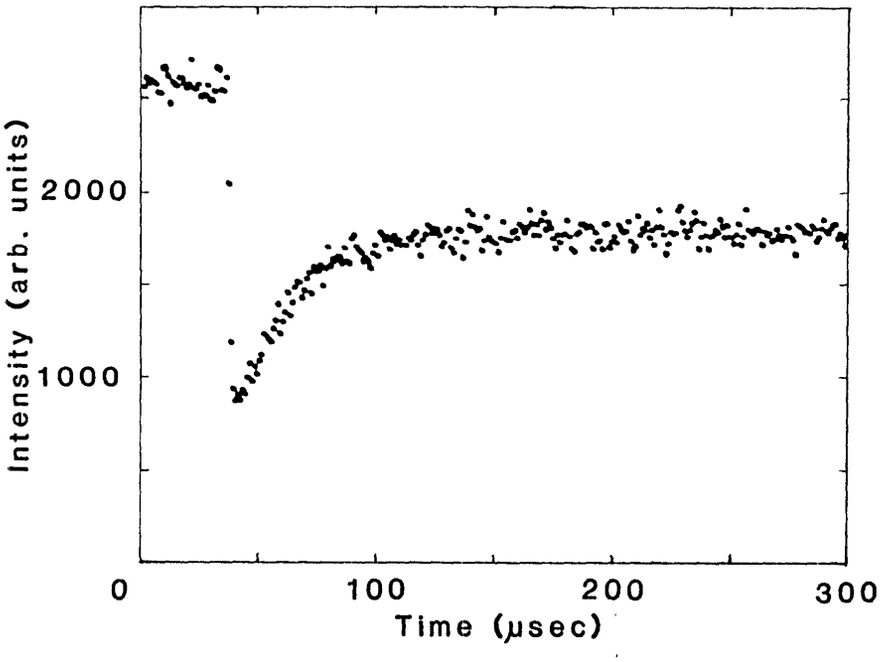

Figure 5.6a *3889 Å intensity regrowth curve for discharge conditions of 250^{0}C oven temperature, 20 Torr helium and 120 mA/anode discharge current. (Each data point represents 1 μsec)*

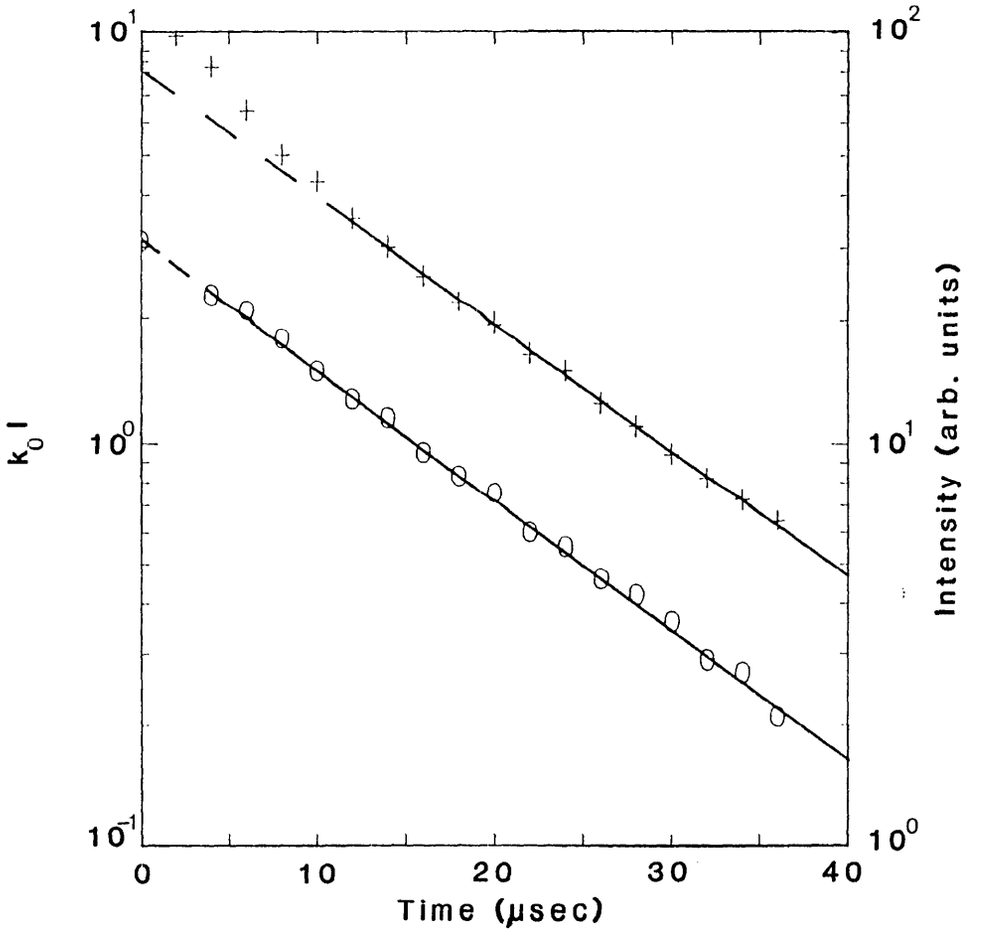

Figure 5.6b *Semi-logarithmic plots of the 4416 Å intensity (+) and the 2^3S metastable density (0) as a function of time after current termination. Discharge conditions as for Figure 5.6a*

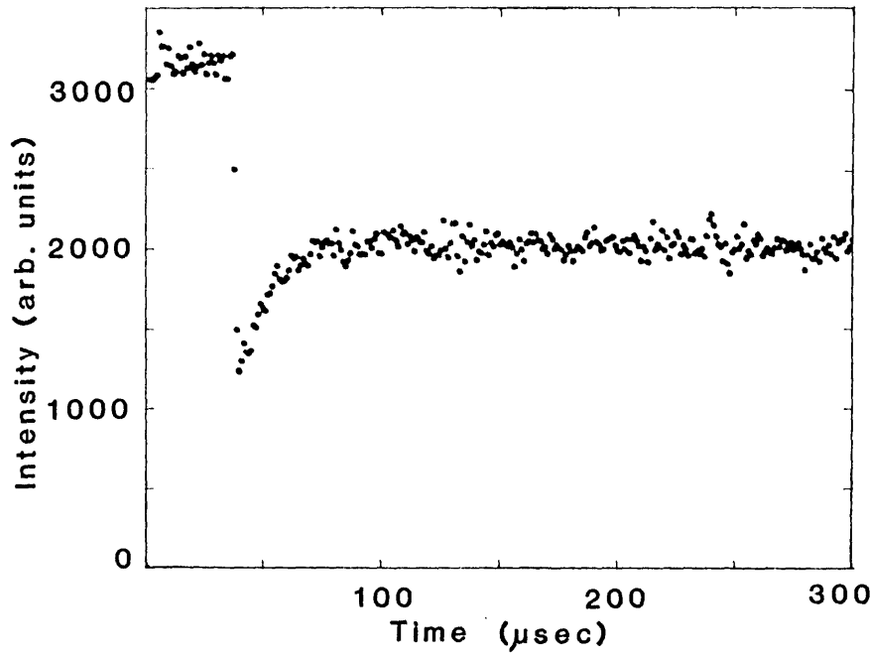

Figure 5.7a *3889 Å intensity regrowth curve for discharge conditions of 275°C oven temperature, 20 Torr helium and 120 mA/anode discharge current. (Each data point represents 1 μsec)*

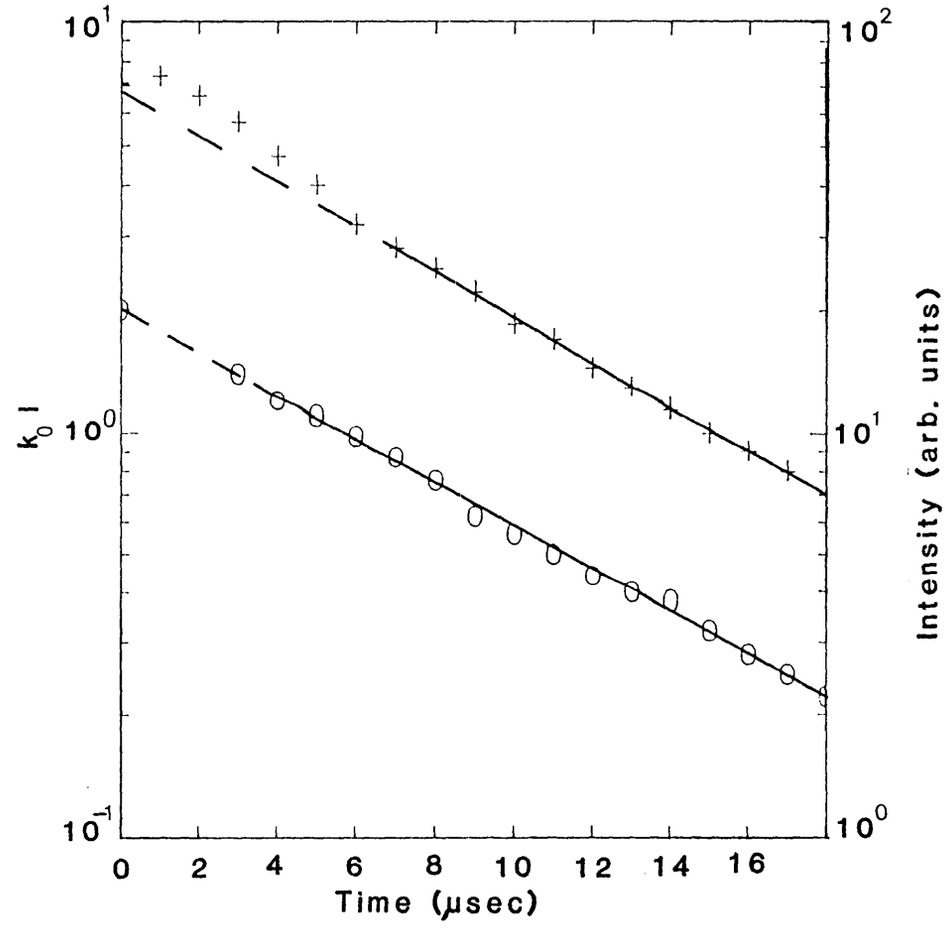

Figure 5.7b *Semi-logarithmic plots of the 4416 Å intensity (+) and the 2^3S metastable density (0) as a function of time after current termination. Discharge conditions as for Figure 5.7a*

study of the intensity regrowth could be made for oven temperatures greater than 275°C because beyond this temperature the density of the He (2^3S) metastable atoms was so small (~100 x less than at 225°C) that absorption was negligible. Further, because of a decrease in the number of energetic electrons due to the presence of a high concentration of low ionization potential metal, the number of helium atoms in levels $>2^1S$, 2^3S also decreases at higher oven temperatures thus lowering the intensity at 3889 Å in particular. The net result of these effects was an increase in the spread of the data points on the intensity regrowth curves and an increased uncertainty in the measured value of Λ_L. In addition, with the resistance value used, the response of the detection system was RC limited to times ~3 μsec which was expected to be of a similar magnitude to the 2^3S metastable decay at an oven temperature of 300°C. In these circumstances the observed intensity regrowth would be convoluted with the instrument response to such an extent that assessment of the actual decay at this oven temperature would be impossible.

Figures 5.5b - 5.7b show the metastable density as a function of time in the afterglow, calculated from the corresponding intensity regrowth curve and the analysis described in section 5.2.2. These data have been graphed on a semi-logarithmic scale to show the nature of the decay. The metastable density has been calculated at times greater than 5 μsec because, only for times greater than this was the signal due solely to that from the emitter.

The 2^3S metastable density decays exponentially with a slope (on a semi-logarithmic plot) which increases with increasing oven temperature. This dependence upon cadmium concentration of the slope is again consistent with Penning collisions and diffusion dominating the late

afterglow loss processes. If this is the case then the experimentally determined slope should be equal to the value calculated from equation (4.3)

$$\text{slope } (\gamma) = N_{Cd} < \sigma_p v > + \frac{D_m}{\Lambda^2 p} \qquad (5.6)$$

Table 5.1 shows a comparison of the experimental values with those calculated from equation (5.6).

TABLE 5.1

OVEN TEMPERATURE ^oC	2^3S DECAY SLOPE FROM EXPERIMENT $(sec)^{-1}$	THEORY $(sec)^{-1}$
225	3.8×10^4	3.8×10^4
250	7.7×10^4	1.1×10^5
275	1.7×10^5	3.1×10^5
300	-	8.3×10^5

In equation (5.6) the value of the diffusion coefficient (D_m) and the Penning collision cross section (σ_p) were taken from Schearer and Padovani (1970) as

$$\sigma_p = 4.5 \times 10^{-15} \text{ cm}^2$$

and

$$D_m = 840 \pm 180 \text{ Torr}^{-1} \text{ cm}^2 \text{ sec}^{-1}$$

where σ_p is the total Penning cross section for the helium 2^3S metastable atoms resulting in excitation of all levels of Cd II.

N_{Cd}, the cadmium neutral density was calculated from

$$N_{Cd} = \frac{9.655 \times 10^{18} \times P_{Cd}\ (\text{Torr})}{T_{tube}\ (\text{K})} \qquad (5.7)$$

where P_{Cd} (Torr) is the cadmium partial pressure calculated from the saturated vapour pressure equation

$$\log_{10} P_{Cd}\ (\text{Torr}) = (-0.2185\ A/T_{oven}\ (\text{K})) + B$$

with $A = 24476.3$

$B = 8.049687$

for $394 < T < 765$ K (Handbook of Chemistry and Physics, 52nd Edition). T_{tube} (K) and T_{oven} (K) refer to the cathode wall and oven sidearm temperatures respectively.

The velocity v appearing in equation (5.6) is the mean relative velocity of the cadmium and helium 2^3S atoms and is given by McDaniel, p.36.

$$v = \left(\frac{8kT_g}{\pi} \right)^{\frac{1}{2}} \left[\frac{1}{M_{He}} + \frac{1}{M_{cd}} \right]^{\frac{1}{2}}$$

where T_g is the gas temperature the values of which are given in Appendix A2. The value for the diffusion length (Λ) calculated for a cylindrical discharge geometry is the same as that used in section 4.5.3.

Table 5.1 shows a clear discrepancy between theory and experiment. Although at 225°C theory and experiment agree, to within experimental uncertainty, for oven temperatures greater than 225°C the experimental

value is smaller than the value expected from theory. The degree of departure increases with increasing oven temperature.

A number of factors influence evaluation of the slope from equation (5.6). Firstly, because the saturated vapour pressure data used in the calculation of the cadmium neutral density, has been applied to a flowing system this could lead to an overestimate of the atom density and consequently to an overestimate of the slope. Secondly, the methods employed to measure and regulate the oven temperature must be questioned. The temperature of the oven was determined using a chromel-alumel thermocouple placed in contact with the external surface of the oven (see Figure A1.4). The heater element was wrapped around the oven and insulated to minimize heat loss. However, the large "Conflat" flange used to access the oven was not directly heated nor well insulated and could thus act as a large radiator. The net result of this could be that the internal temperature of the oven would not acquire the temperature of the external surface which was the point of temperature measurement. Thus, using the oven temperature determined in the manner just described could give rise to an overestimate of the cadmium partial pressure and hence an overestimate in the value of the slope calculated from equation (5.6).

To examine the effect of the thermocouple position on the 2^3S metastable density decay rate, the 3889 Å intensity regrowth was recorded for a number of thermocouple positions on the sidearm. Upon analysis of the data it was clear that the measured decay rate was a strong function of thermocouple position with the best results (those presented in Table 5.1) being obtained when the thermocouple was positioned at the coldest point on the sidearm (at the junction between the sidearm and the

flange). In view of the fact that the flange was cooler than the sidearm and that a small variation in the oven temperature produces a marked effect on the cadmium partial pressure it is clear that the discrepancies between theory and experiment could be due, in part, to the oven not acquiring the temperature as measured on the outer surface of the sidearm.

Another possible source of error could be that the discharge responded only slowly to a change in oven temperature. Under normal operation a period of at least 1 hour was allowed for the system to achieve equilibrium following a small change in oven temperature. To investigate whether this time was sufficient the decay of the 2^3S metastable atoms was measured every hour for three hours following a temperature change. Over this time period no change in the slope was observed indicating that the thermal response time of the system was not a limiting factor in the experiment.

It was observed by Grace (1978) that the value of the metastable density was a function of the helium gas flow through the discharge. This was attributed by him to a lowering of the cadmium concentration with an increase in the helium flow rate. Although no mechanism was proposed to explain this phenomenon, it was believed to be associated with the faster sweep out rate of the cadmium from the discharge. However, on the basis of the present study an alternative mechanism can be proposed being that, increases in the flow of a cold gas result in an increased heat loss from the oven region and consequently a slight lowering of the oven temperature and hence to a reduction in the cadmium partial pressure. Although there is no direct evidence to support this a similar, though more dramatic, phenomenon was observed in an identical He-Sr hollow cathode discharge (Brown, 1983) where cooling of the oven,

now being operated at $\backsim 650^{o}C$, was so great that Sr condensed in the gas flow region eventually stopping gas flow.

5.4.2 Comparison with the 4416 Å Decay

As the main aim of this study is to establish the role of the metastable atoms in populating the upper level of the 4416 Å Cd II transition late in the afterglow, the corresponding 4416 Å decay curves are also shown in Figures 5.5b - 5.7b and numerical values of the slope of the 4416 Å intensity are compared with those of the 2^3S metastable decay in Table 5.2.

TABLE 5.2

OVEN TEMPERATURE ^{o}C	4416 Å DECAY SLOPE $(sec)^{-1}$	2^3S METASTABLE DECAY SLOPE $(sec)^{-1}$
225	3.8×10^4	3.8×10^4
250	7.5×10^4	7.7×10^4
275	1.9×10^5	1.7×10^5

Table 5.2 shows that the slope of the 4416 Å decay agrees with the decay of the 2^3S metastable density to within experimental uncertainty. This agreement is the evidence required to link the mechanism populating the $5s^2\ ^2D_{5/2}$ level of Cd II late in the afterglow to that of a Penning collision between the helium 2^3S metastable atoms and cadmium neutral atoms.

5.4.3 Variation with Oven Temperature of the Decay of the 2^1S Density

The 2^1S metastable density decay was calculated from measurements of the intensity regrowth of the 5016 Å transition. Results showing the intensity regrowth for oven temperature values of 225°C, 250°C and 275°C are shown in Figures 5.8a - 5.10. Because of the very rapid decay rates and a decrease in the amount of absorption no experimental results for oven temperature values greater than 275°C could be recorded.

Following the analysis of section 5.2 the corresponding 2^1S metastable density as a function of time in the afterglow is graphed, on a semi-logarithmic scale, in Figures 5.8b and 5.9b. On the same diagrams are graphed the 2^3S metastable density evaluated under identical discharge conditions and it is clear that the singlet metastable species is destroyed more quickly than the triplet. (Because of the rapid decay at an oven temperature of 275°C it was not possible to accurately calculate the 2^1S population at this temperature.)

As the cross section for the destruction of the He (2^1S) atoms via Penning collisions is of the same magnitude as that for the triplet metastable species (Collins et al., 1971) the experimental result suggests that another collision process is responsible for the rapid decay of the singlet species in the afterglow. This mechanism is thought to be that of singlet to triplet metastable conversion, represented by

$$He\ (2^1S) + e_{slow} \longrightarrow He\ (2^3S) + e_{fast} \qquad (5.8)$$

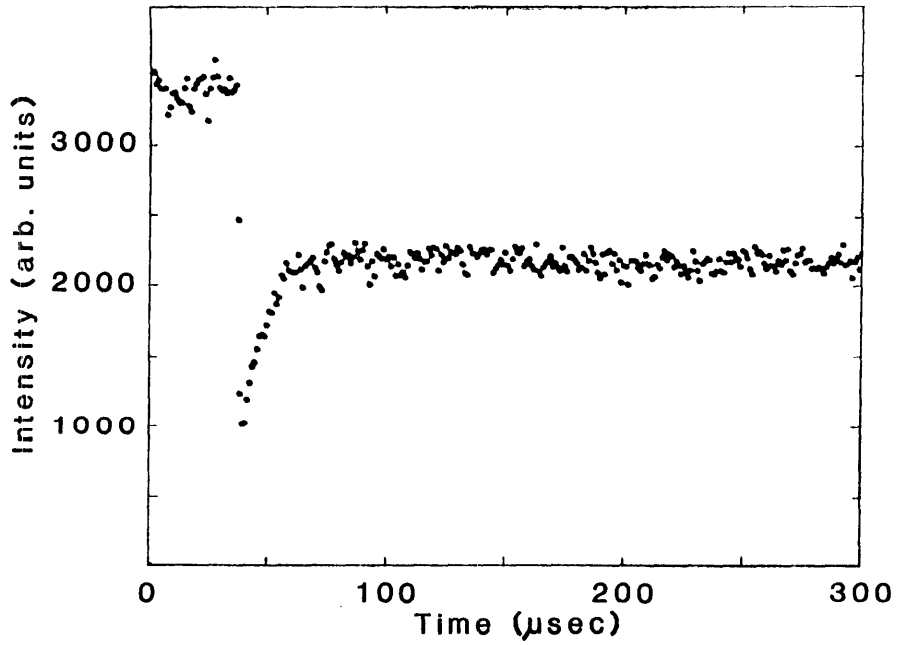

Figure 5.8a *5016 Å intensity regrowth curve for discharge conditions of 225°C oven temperature, 20 Torr helium and 120 mA/anode discharge current. (Each data point represents 1 μsec)*

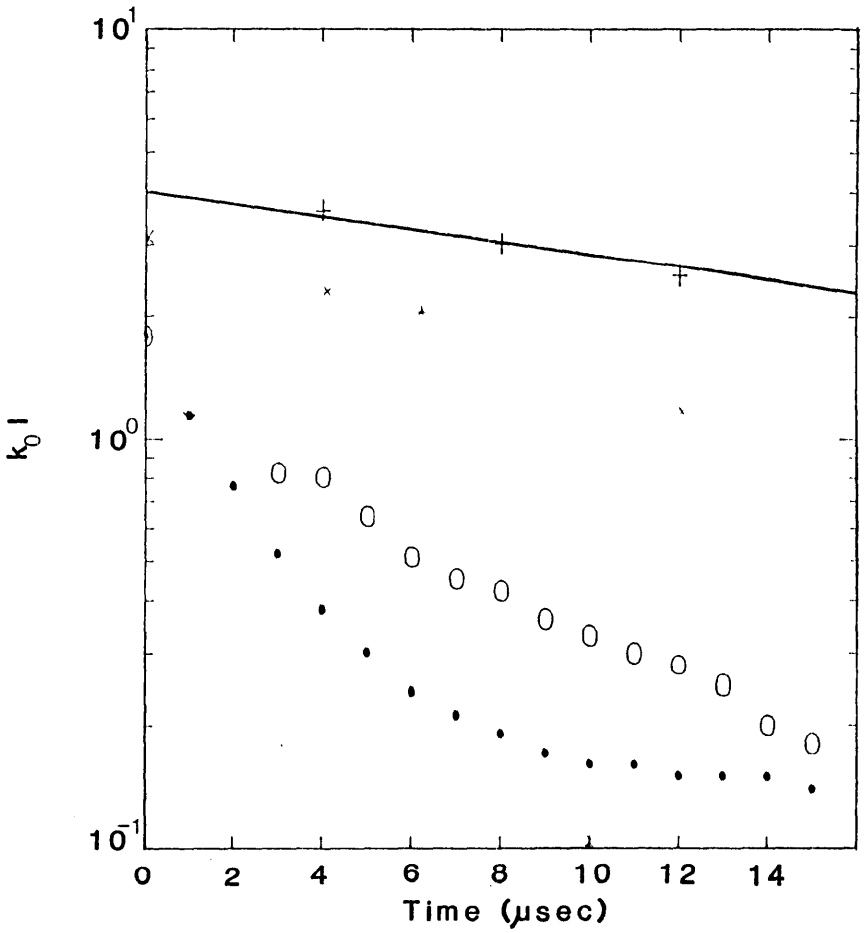

Figure 5.8b *Semi-logarithmic plots showing the 2^3S (+) and 2^1S experimental (0) and theoretical (•) density decay in the afterglow. Discharge conditions as for Figure 5.8a*

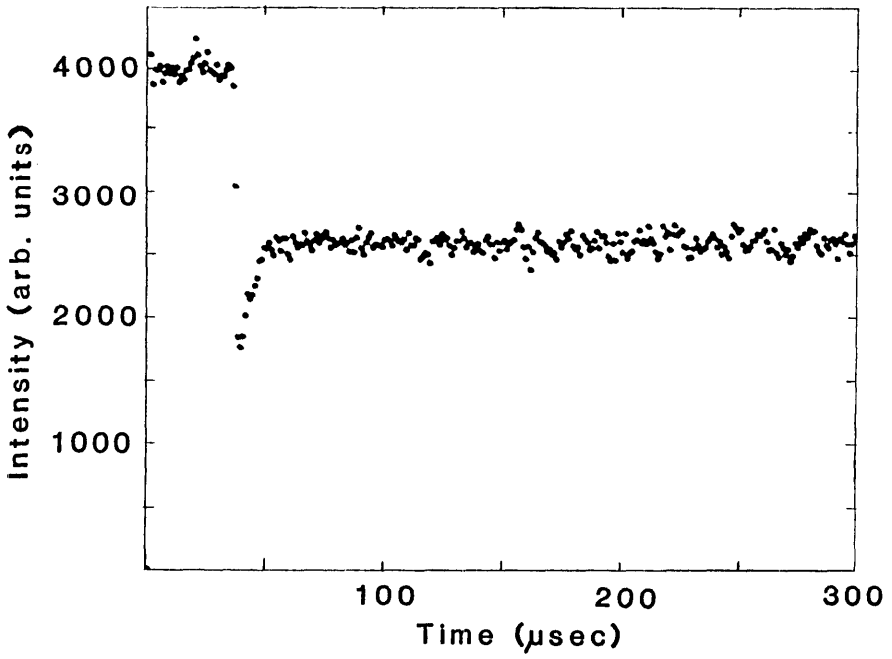

Figure 5.9a *5016 Å intensity regrowth curve for discharge conditions of 250°C oven temperature, 20 Torr helium and 120 mA/anode discharge current. (Each data point represents 1 μsec)*

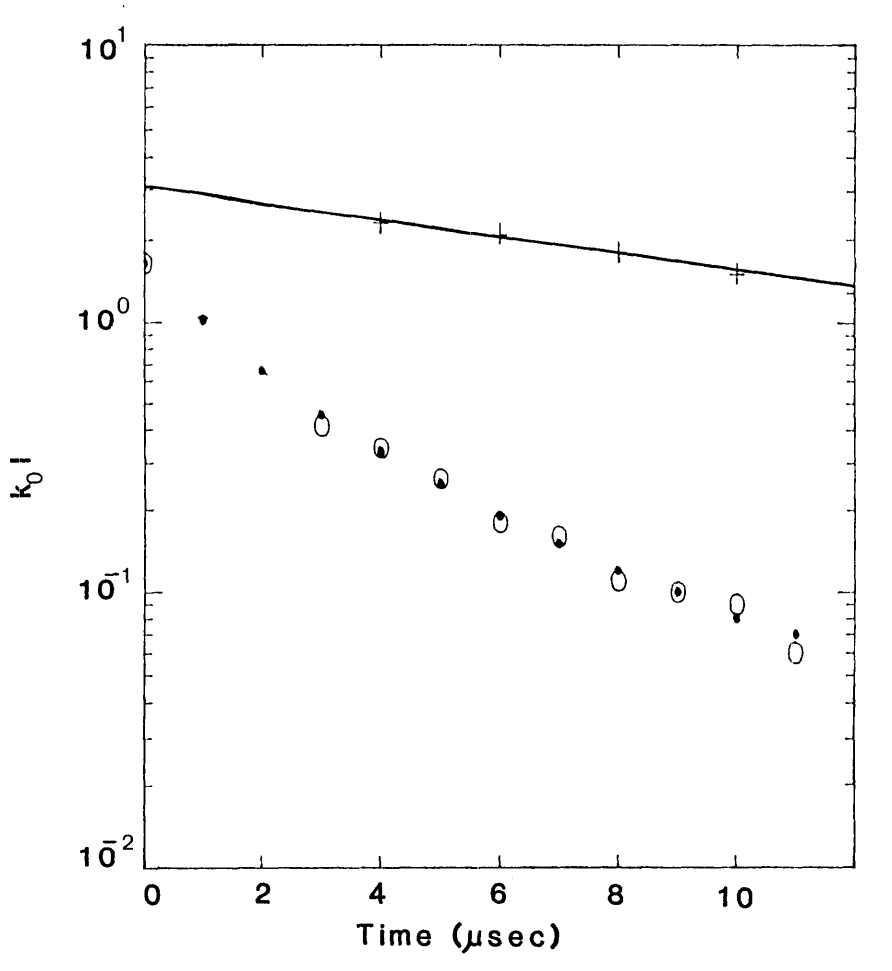

Figure 5.9b *Semi-logarithmic plots showing the 2^3S (+) and 2^1S experimental (o) and theoretical (•) density decay in the afterglow. Discharge conditions as for Figure 5.9a*

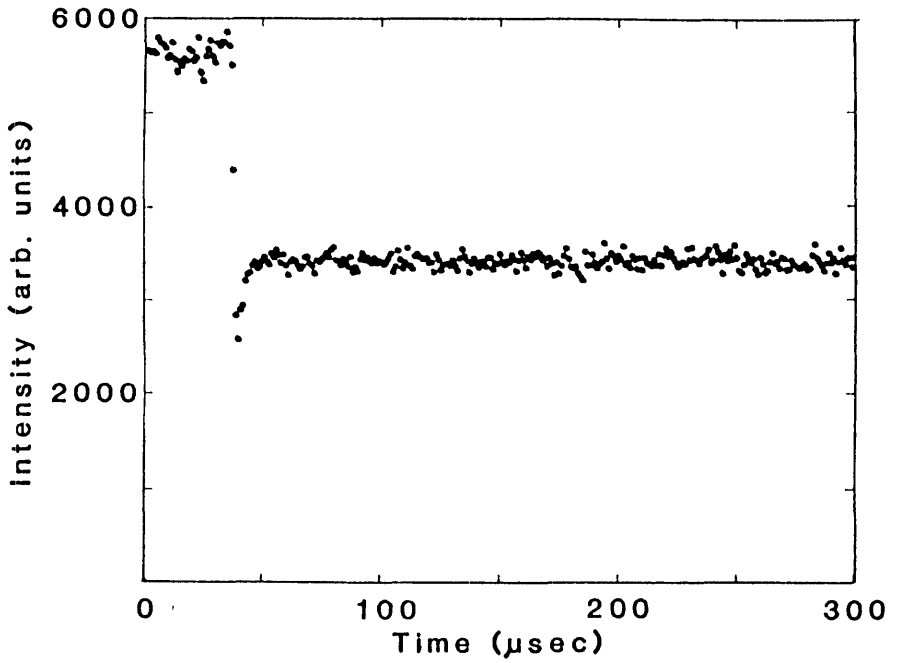

Figure 5.10 5016 Å intensity regrowth curve for discharge conditions of 275 C oven temperature, 20 Torr helium and 120 mA/anode discharge current. (Each data point represents 1 usec)

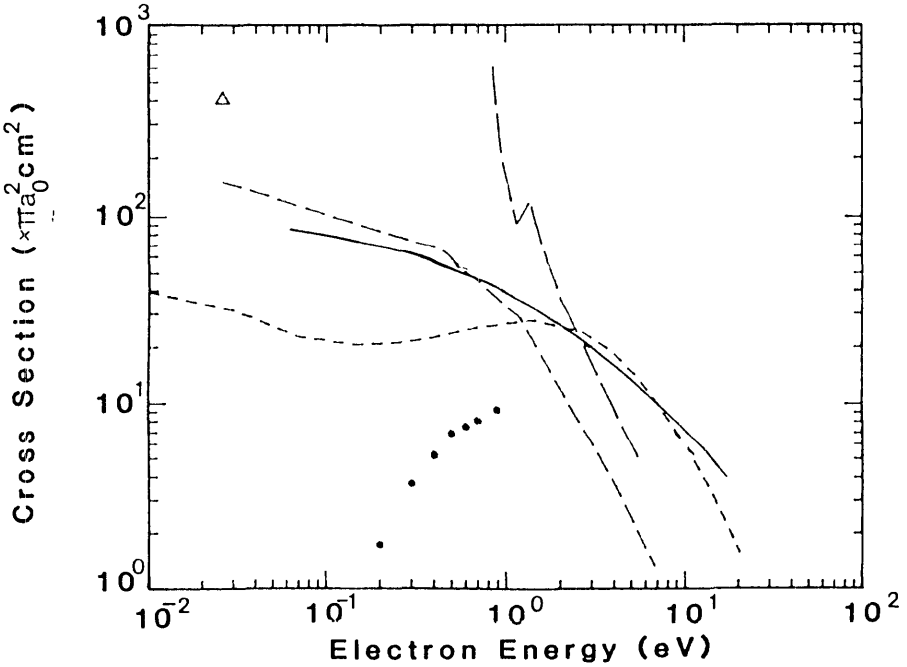

Figure 5.11 Comparison of available experimental and theoretical cross section data for singlet to triplet metastable conversion

——— *Fujimoto (1978)*

—— —— *Burke et al (1969)*

— — — — *Marriott (1966)*

- - - - - - *Morrison and Rudge (1967)*

• *Gerasimov and Startsev (1974)*

Δ *Phelps (1955)*

If this is the case, in the afterglow the rate equation for the 2^1S density can then be written as

$$\frac{dN\ (2^1S)}{dt} = -(N(2^1S) \cdot N_{Cd} < \sigma_p^s v > + N(2^1S) n_e(t) < \sigma_{2^1S-2^3S} v >) \quad (5.9)$$

where $N(2^1S)$ and $n_e(t)$ are the 2^1S and electron densities in the afterglow, $< \sigma_p^s v >$ is the rate coefficient for Penning collisions and $< \sigma_{2^1S-2^3S} v >$ is the rate coefficient for singlet to triplet conversion. In equation (5.9) no account has been made for the reverse process

$$He\ (2^3S) + e \rightarrow He\ (2^1S) + e \quad (5.10)$$

which is expected from detailed balancing. The rate coefficient for reaction 5.10, $< \sigma_{2^3S-2^1S} v >$ is related to that of reaction 5.8 by

$$< \sigma_{2^3 3-2^1S} v > = \frac{g_u}{g_l} < \sigma_{2^1S-2^3S} v > \exp\left[-\chi/kT_e\right] \quad (5.11)$$

where g_l and g_u are the statistical weights of the 2^3S and 2^1S levels respectively, χ is the threshold energy of excitation and T_e is the electron temperature. Since χ has a value of $\sim$0.6 eV and $kT_e << \chi$ in the afterglow then

$$< \sigma_{2^3S-2^1S} v > \quad << \quad < \sigma_{2^1S-2^3S} v >$$

and triplet to singlet conversion can be neglected.

The cross section for singlet to triplet conversion has not been extensively studied. The available experimental (Phelps, 1955; Gerasimov and Startsev, 1974) and theoretical (Marriott, 1966; Morrison and Rudge, 1967; Burke et al., 1969) results are shown in Figure 5.11. Also shown

is the collision cross section calculated from the semi-empirical formula of Fujimoto (1978). The analytical approximation of Fujimoto is in general agreement with the quantum mechanical calculations of Marriott (1966) and Burke et al. (1969) and the experimental results of Phelps (1955), and is in a form which permits ease of calculation of the rate coefficient for the electron energy range of interest.

From Fujimoto, the collision cross section for 2^3S to 2^1S conversion is represented by

$$\sigma(U) = 28\pi\, a_0^2 \left(\frac{U-1}{U}\right) \text{ cm}^2 \qquad (5.12)$$

where $U = \xi/\chi$ and ξ is the energy of the colliding electron and χ the energy difference between the states. The corresponding collision rate coefficient was calculated from

$$\langle \sigma_{2^3S-2^1S} v \rangle = \left(\frac{2e}{m}\right)^{\frac{1}{2}} \int_{-\infty}^{\infty} \sigma(\xi)\, \xi^{\frac{1}{2}}\, f(\xi)\, d\xi$$

where $f(\xi)$, the electron energy distribution function, was assumed to be Maxwellian. The rate coefficient for singlet to triplet conversion is then obtainable from detailed balancing using equation (5.11).

Using the value of N_{Cd} as calculated in section 5.4.1, $\sigma_p^s = 1 \times 10^{-14}$ cm^2 (Collins et al., 1971), the initial 2^1S density calculated from absorption (chapter 3) and $n_e(t)$ using the approximation outlined in Chapter 7, the decay of the 2^1S density in the afterglow was calculated from equation (5.9) using a computer based numerical differential technique.

However, using this simple model the predicted decay was much too rapid at times late in the afterglow suggesting that some production

mechanism was becoming important in this region. As the process of triplet to singlet conversion was ruled out the only other possibility would be that of recombination of a helium ion leading to the formation of a helium atom in the singlet metastable level, i.e.

$$He^+ + e + e \rightarrow He\ (1^1S_0) + e$$

Addition of recombination to the rate equation gives

$$\frac{dN(2^1S)}{dt} = -(N(2^1S)\ N_{Cd} < \sigma_p^s v > + N(2^1S)\ n_e(t) < \sigma_{2^1S-2^3S}\ v > + k\ \alpha\ n_e^2(t)\ N(He^+) \qquad (5.13)$$

where α is the recombination coefficient and k an adjustable parameter representing the number of recombining ions resulting in the formation of a 2^1S atom. On the basis of the statistical weights it was thought that recombination would go as 3:1 for production of 2^3S and 2^1S levels respectively and thus a value of k = 0.25 was used.

Using the recombination coefficient discussed in section 6.4.1 and the initial helium ion density estimated in Chapter 3, equation (5.13) was evaluated and the results of these calculations are shown in Figures 5.8b - 5.9b. In view of the large degree of uncertainty associated with many of the parameters used in evaluating equation (5.13), the good agreement between theory and experiment is probably fortuitous.

Results of these calculations indicate that while singlet to triplet conversion is the dominant loss mechanism at low oven temperatures this is not necessarily true at higher temperatures. Increasing the cadmium concentration increases the Penning collision rate and although the electron temperature falls its effect on the knockdown rate will be minimal. Thus Penning collisions will begin to play a more important

role in the 2^1S decay at higher oven temperatures.

5.5 SUMMARY

In this chapter, afterglow studies of the decay of the He (2^3S) and He (2^1S) metastable species were presented. These experiments were essential in order to provide conclusive evidence proving that, at least in the late afterglow, the Penning ionization mechanism is the sole collision process by which the $5s^2\ ^2D_{5/2}$ level is populated. Measurements were made using the Ladenburg-Reiche line absorption method and experimental data were obtained showing the decay of the singlet and triplet metastable species as a function of the cadmium neutral density. No additional information was obtained from a study of the current and pressure dependence of the decay of these species because of the low signal levels from the transitions investigated and hence the poor quality of the data even after signal averaging and processing.

Results of this investigation showed conclusively the dominant role of Penning ionization in populating the upper level of the 4416 Å Cd II transition in the late afterglow. This conclusion was based on two main observations: firstly, under all experimental conditions the 2^3S decay was exponential with a time constant that increased with the cadmium concentration (oven temperature) and secondly, the excellent agreement between the late afterglow 4416 Å spontaneous emission decay and the corresponding decay of the He (2^3S) density.

To provide further confirmation, the decay of the metastable species was modelled using a simple theory accounting only for He (2^3S) destruction via diffusion and Penning collisions. It was found, however,

that the theoretical predictions and experiment agreed only at low oven temperatures and showed significant discrepancies as the oven temperature was increased. This inconsistency was eventually attributed to the method used to heat the oven sidearm and, in particular, it is suggested that the oven temperature and hence cadmium density are significantly lower than those calculated from the temperature measurements of the externally placed thermocouples. An attempt was made to confirm this result through direct measurement of the cadmium neutral density (reported in Appendix A3) and, while the experimental values of N_{Cd} were much less than those derived using saturated vapour pressure data and the oven sidearm and cathode wall temperatures, the discrepancy was so large that it suggested the experimental method needs more careful consideration before any confidence could be ascribed to the results.

Investigation of the He (2^1S) decay provided significant insight into the role of the slow thermal electrons in the early afterglow. The measured 2^1S decay was found to be much more rapid than that of the corresponding 2^3S density. This was explained in terms of singlet to triplet metastable conversion providing the major pathway for singlet metastable destruction in the afterglow of the hollow cathode discharge. This result provides direct confirmation of the role of collisions of the second kind in the early afterglow and suggests that similar processes could explain the early afterglow characteristics of the 4416 Å decay.

Since the initial, or steady state, singlet metastable density is a significant fraction of the triplet density, one might expect that, as a result of singlet to triplet conversion, the triplet density would show a corresponding increase in the early afterglow. This feature was not observed with the present apparatus. The reason for this was that, in

order to achieve adequate signal to noise characteristics of the experimental data, the response time of the detector/data acquisition system was reduced. In fact, the response time of the apparatus was such that only the gross features of the decay were evident and the transient or relatively short time events, such as the effect of singlet to triplet conversion, were averaged out. The difficulty experienced in determining the zero intensity level also contributed to this dilemma.

CHAPTER 6

INVESTIGATION OF THE EARLY AFTERGLOW COLLISION MECHANISMS

6.1 INTRODUCTION

The afterglow of the He-Cd^+ hollow cathode discharge was investigated in order to provide an unambiguous test of the original hypthesis, viz that the Penning collision process alone is responsible for populating the $5s^2\ ^2D_{5/2}$ level of Cd II. Results of this investigation, showing the parametric variation of the 4416 Å spontaneous emission decay and the decay of the He (2^3S, 2^1S) densities, were presented and discussed in Chapters 4 and 5 respectively.

The decay of the 4416 Å spontaneous emission, shown again in Figure 6.1, was more complex than anticipated. Although in Chapter 5 the late afterglow collision process resulting in the excitation of the $5s^2\ ^2D_{5/2}$ upper level of the 4416 Å Cd II transition was shown to be the Penning collision mechanism, no obvious explanation could be proposed to account for the early afterglow intensity increase and subsequent rapid decay.

Some indication of the complexity of the collision processes in the early afterglow was obtained from a closer examination of the systematic variations in the nature of the 4416 Å decay with discharge current and helium pressure. From these observations, in particular that of the current and pressure dependence of the point of intersection of the extrapolated exponential tail with the afterglow initiation axis (reported in sections 4.5.2 and 4.5.3), it was concluded that electronic

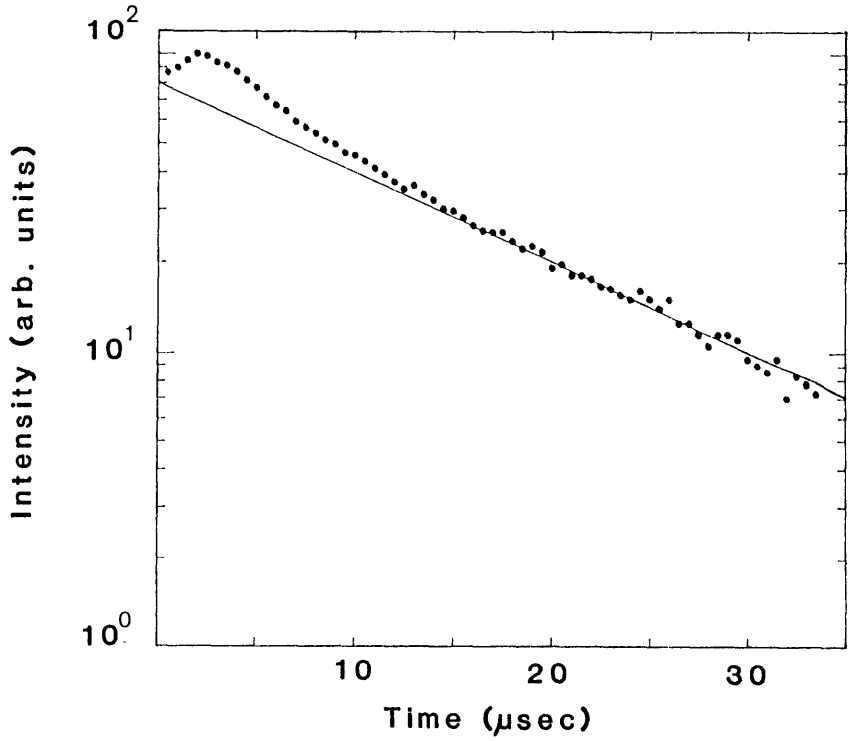

Figure 6.1 4416 Å spontaneous decay for an oven temperature of 250^{0}C, 20 Torr helium and 120 mA/anode discharge current

processes contribute significantly to the decay in the early afterglow. On the other hand the observation of an inverse current dependence of the relative peak height (section 4.5.2) was interpreted as implying that the $5s^2\ ^2D_{5/2}$ population is not directly affected by these processes.

The role of the thermalized electrons in the early afterglow was later confirmed from measurements of the decay of the He (2^1S) metastable density. This species was observed to decay rapidly in the afterglow, much more rapidly than the He (2^3S) density, a result which could only be explained if singlet to triplet metastable conversion via collisions of the second kind is the dominant loss mechanism for the helium singlet metastable species in the afterglow.

Interpretation of the available experimental data is complicated by the complex, and as yet uninvestigated, early afterglow region of a He-Cd^+ hollow cathode discharge. On the other hand, the afterglow of the He-Cd^+ positive column discharge has been investigated. Goto (1982), who obtained similar curves to those of the present study, interpreted the fact that the point of intersection of the late afterglow exponential tail with the afterglow initiation axis was at a value lower than that of the d.c. intensity as evidence to support the view that electronic excitation plays an important role in populating the $5s^2\ ^2D_{5/2}$ level. This is perhaps a surprising conclusion in view of the fact that the early afterglow decay has a time constant much too long to be associated with the cessation of electronic excitation processes (typically 1-2 μsec). Goto, who obtained his results by photographing oscilloscope traces, did not observe an intensity increase.

In view of the apparent complexity of the early afterglow region and the desire to utilize the afterglow data to confirm the previous conclusions based on observations in the d.c. discharge, some attempt must be made to identify the mechanisms active in this region. This chapter addresses this problem through both experimental observations, wherever possible, and theoretical calculations.

To explain the variations in the 4416 Å intensity in the early afterglow a number of possible mechanisms are proposed and investigated, namely:

1. that the excited state cadmium ion densities are not distributed uniformly across the tube diameter and, in particular, have a depression along the discharge axis so that redistribution of these species in the early

afterglow results in an increase in the $5s^2\ ^2D_{5/2}$ density within the central discharge region and consequently results in the observed intensity increase in the early afterglow;

2. that the early afterglow characteristics of the 4416 Å spontaneous emission are due to changes in the $5s^2\ ^2D_{5/2}$ level as a result of slow electron collisions redistributing the populations of the higher lying Cd II levels, in particular the $5s^2\ ^2D_{3/2}$ level;

3. that there is a significant fraction of Cd^{++} produced in the d.c. discharge which through recombination and subsequent cascade to the $5s^2\ ^2D_{5/2}$ level of the cadmium ion could result in an increase of the $5s^2\ ^2D_{5/2}$ population in the early afterglow;

and,

4. that the $5s^2\ ^2D_{5/2}$ level is populated solely by Penning collisions in the afterglow and thus the 4416 Å spontaneous decay simply follows that of the He (2^3S) metastable density.

In this chapter each of these plausible mechanisms is investigated and the results of the study presented and discussed.

In section 6.2, results of radial profile studies of the Cd II densities in the d.c. hollow cathode discharge are presented. Radial profiles of the Cd II ground and excited state densities are inferred from investigation of the radial dependence of the 4416 Å spontaneous emission. For these studies an optical system was designed so that only a small cylindrical discharge region was viewed by the detection system. This viewing region was subsequently scanned across the discharge

diameter. Results of this investigation showed that, except at high helium pressures, the Cd II density has an axial maximum, decreasing monotonically to the tube walls. The results were in agreement with those of Gill and Webb (1978) for a hollow cathode He-Zn^+ discharge. On the basis of these experimental results, it was thus concluded that the existence of non uniform Cd II density profiles did not explain the observed characteristics of the 4416 Å spontaneous emission.

The importance of collisional redistribution of the higher lying Cd II levels in populating the $5s\ ^2\ ^2D_{5/2}$ level is assessed in section 6.3. Particular consideration was given to discussion of electronic relaxation of the $5s^2\ ^2D_{3/2}$ level. As the interaction potential involves long range Coulomb forces and the level lies approximately leV above the $5s^2\ ^2D_{5/2}$ level requiring only a J changing collision of the electron, the rate coefficient for this process may be expected to be large. This, coupled with expected large initial electron and $5s^2\ ^2D_{3/2}$ densities could result in the transfer $J = 3/2 \longrightarrow 5/2$ being of the same magnitude as that of the radiative lifetime of the $5s^2\ ^2D_{3/2}$ level. The role of electronic redistribution of the Cd II levels is difficult to assess either experimentally or theoretically because of the complexity of the afterglow and limited knowledge of the collision cross sections and electron energy distributions. However, from the observation of the inverse current dependence of the relative peak height of the 4416 Å decay it is argued that these processes are not significant in the early afterglow.

Recombination of Cd^{++} and the subsequent decay to the $5s^2\ ^2D_{5/2}$ level is considered in section 6.4. Because of the existence of a large number of high energy electrons in the d.c. discharge coupled with the

fact that the Cd^{++} ground state lies only 25.9 eV above the Cd ground state (whereas He^{+} is 24.6eV above He ground state) the existence of a large Cd^{++} population in the d.c. discharge cannot be overlooked. Despite this fact, careful spectroscopic examination of the He-Cd^{+} hollow cathode discharge showed no evidence to support the view that Cd^{++} is a significant ionic species in these discharge types and, more significantly, the observed inverse current dependence of the relative peak height is not indicative of recombination processes. Thus it is argued that this process does not offer a plausible explanation of the early afterglow characteristics of the 4416 Å spontaneous decay.

Lastly, if it is proposed that the Penning collision process is the sole excitation mechanism of the $5s^2\ ^2D_{5/2}$ level in the afterglow then processes which directly influence the metastable density in the early afterglow must be considered. While the experimental results of Chapter 5 suggest that the 2^3S metastable decay is determined solely by Penning collisions and diffusion, experimental difficulties were such that no accurate data for the evolution of this species in the early afterglow could be obtained and thus, no direct experimental evidence supporting the proposed mechanism was obtained. In section 6.5 the processes which can directly affect the He (2^3S) density in the afterglow are explored. These processes include:

1. recombination of He^{+};
2. slow electron collisions and/or radiative decay from higher lying helium levels;
3. electronic relaxation of He (2^3S) to the ground state.

Through comparison of the temporal evolution of selected helium

spectral lines in both the helium and helium-cadmium afterglow (section 6.5.1) it is shown that recombination is not a significant process in the afterglow of the He-Cd discharge. The efficiency of the remaining two mechanisms could only be assessed through theoretical calculations involving knowledge of both the collision cross sections for the various processes as well as the electron energy distribution function in the afterglow. Direct confirmation of the role of the slow electrons in the afterglow was obtained from a measurement of the 2^1S decay which was shown to be dominated by $2^1S \longrightarrow 2^3S$ conversion.

Results of these calculations (sections 6.5.2 and 6.5.3) indicated that, in the early afterglow region where the electron density is large, the 2^3S level is populated by electronic relaxation and radiative decay of the higher lying states and destroyed through electronic deactivation to the ground state, Penning collisions and diffusion. Thus the inclusion of these additional processes in the description of the early afterglow may conceivably give a plausible explanation of the early afterglow characteristics of the 4416 Å decay. This study is the subject of Chapter 7.

6.2 RADIAL PROFILES OF THE CADMIUM ION EXCITED STATE DENSITIES

Figure 6.2 shows a sketch of a possible radial distribution of excited cadmium ions in the discharge. Although such a distribution has been observed by Gill and Webb (1978) only at high helium pressures in a $He-Zn^+$ hollow cathode discharge, we cannot exclude the possibility that such a distribution might occur at lower pressures in $He-Cd^+$. If so,

then redistribution of the $(Cd^+)^*$ might produce the intensity peak and non-linear decay at times early in the afterglow.

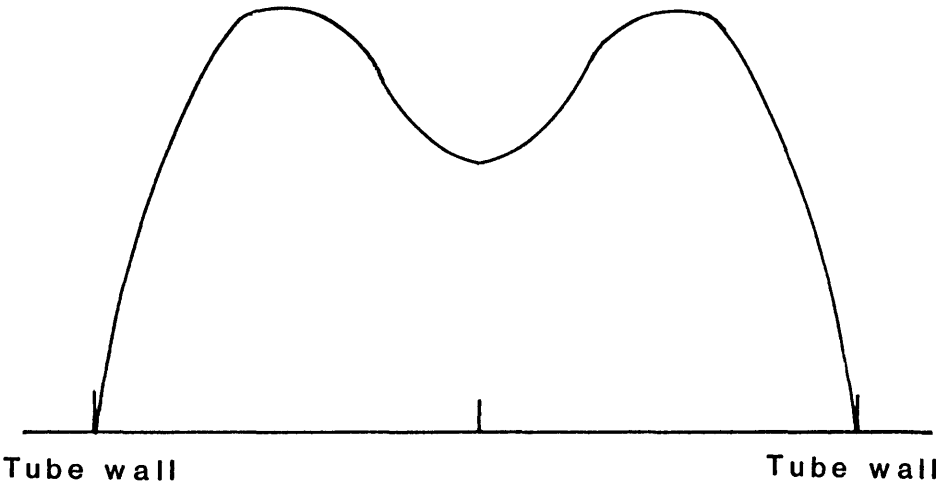

Figure 6.2 A sketch of a possible radial distribution of excited cadmium ions

Figure 6.3 shows the arrangement used for the measurements of the radial profiles of emission lines. The optical system, which was based on the design of Webb (1968), consisted of two apertures S_1 and S_2 and a lens L which permitted only emission from within a narrow cylindrical volume of the discharge to reach the spectrometer. Pinhole S_2 is positioned so that it lies in the plane of the image of the rear plasma element (Σ_1). Similarly S_1 is positioned to coincide with the image of Σ_2 corresponding to the front end of the plasma element. For a

cylindrical region of diameter a, the size (g_2) of the pinhole S_2 must be

$$g_2 = \frac{V_1}{U_1} a$$

where V_1 and U_1 are the image and object distances shown in Figure 6.3. The size g_1 of pinhole S_1 is determined not by ray optics but by diffraction limitations as

$$g_1 = \frac{V_2}{U_2} \left(a - \frac{1.22\lambda D}{a}\right)$$

where λ is the wavelength of the radiation and D is the length of the discharge region studied.

In order to obtain adequate resolution and intensities the diameter of the plasma cylinder was chosen to be a = 600 μm. The minimum distance between the lens (L) and the plane Σ_2, determined by the discharge tube design was U_2 = 40 cm and a quartz lens of 5 cm diameter and focal length of 30 cm was used as the lens (L). With this geometry the required pinhole sizes were calculated to be g_1 = 400 μm and g_2 = 600 μm for λ = 4416 Å radiation and a discharge length of 30 cm. Although the pinhole diameters need to be changed with wavelength, this was not done in the present experiment since only signals at 4416 Å were investigated.

In previous studies (Webb, 1968; Gill and Webb, 1978), the radial profiles were determined by lateral tracking of the discharge tube across the optical system. This was impractical with the present apparatus and so the mirror M, shown in Figure 6.3, was positioned so that light from the viewing region was rotated through 90° with respect to the discharge axis. Lateral tracking of the mirror perpendicular to the axis of the

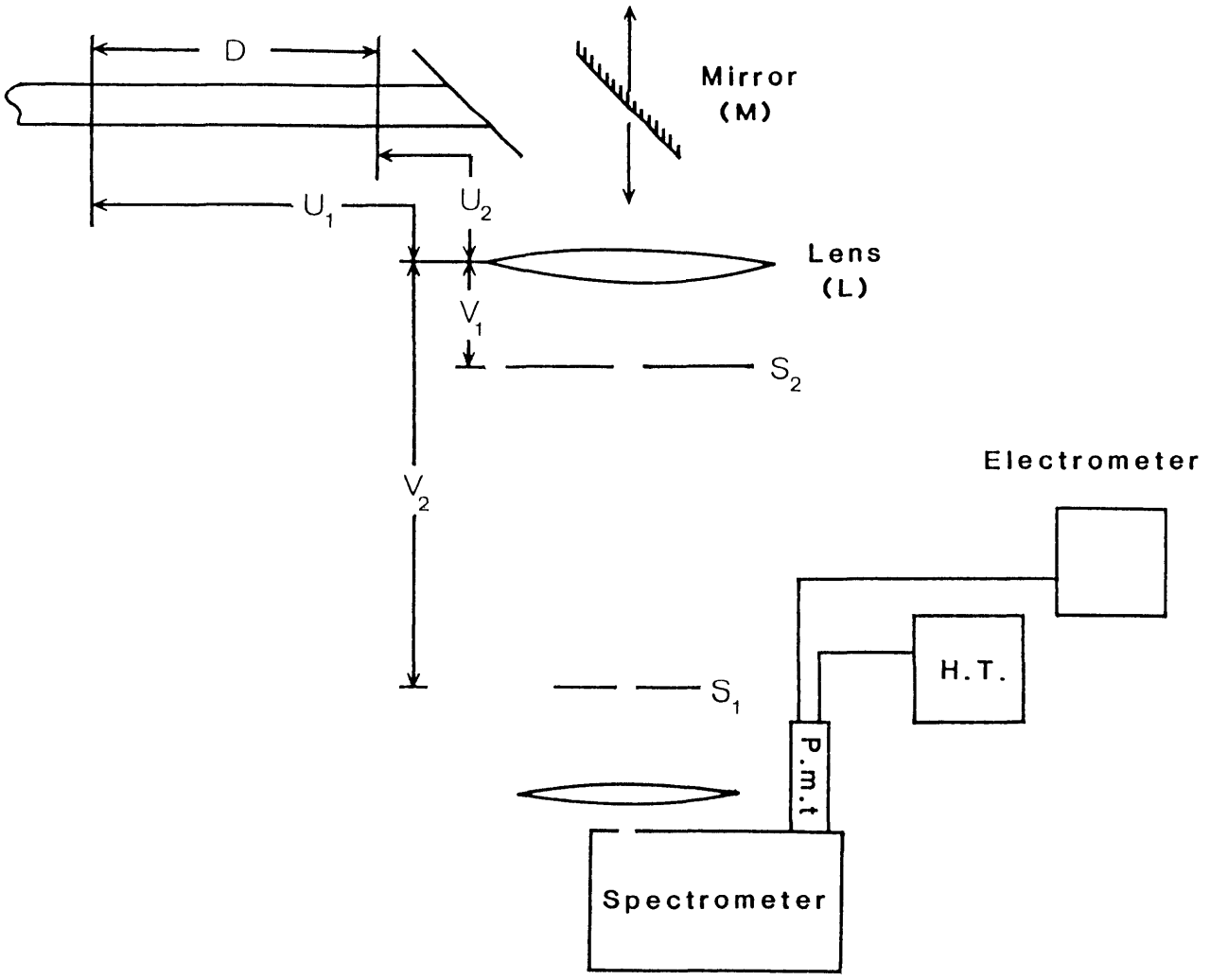

Figure 6.3 A schematic diagram of the experimental arrangement used for the measurement of the radial profiles of emission lines

discharge, and in the plane of the detectors, translated the viewing region across the tube diameter.

The alignment procedure for the optical system was identical to that described in Chapter 3 with only slight modifications to allow for the additional optical elements.

Although the lifetime of the $5s^2\ ^2D_{5/2}$ level is relatively long (~780 nsec), at the helium pressures used in this present study ambipolar diffusion is not expected to be a significant loss process and thus, a study of the 4416 Å spontaneous emission should provide information concerning the steady state radial distribution of cadmium ions in this level.

Results of the experiment showing the 4416 Å radial intensity as a function of discharge current, helium pressure and oven temperature are shown in Figures 6.4 - 6.6. These results are in good agreement with those of Gill and Webb (1978) and clearly show that for normal operating parameters the excited ion densities have an axial maximum, decreasing monotonically to the wall. Only for high helium pressures ($p > 35$ Torr) does the $5s^2\ ^2D_{5/2}$ distribution begin to acquire the profile shown in Figure 6.2.

In the light of this investigation, it is apparent that the presence of non-uniform radial profiles of excited Cd ions cannot provide an explanation for the observed intensity peak in the early afterglow of the 4416 Å decay.

With the radial scan apparatus set up, it was opportune to check that the 4416 Å decay was independent of radial position. The results, showing the 4416 Å decay for three different radial positions are presented in Figure 6.7. Although the quality of the data is poor, due to the low signal levels received at the detectors, the results revealed that the 4416 Å decay is independent of radial position.

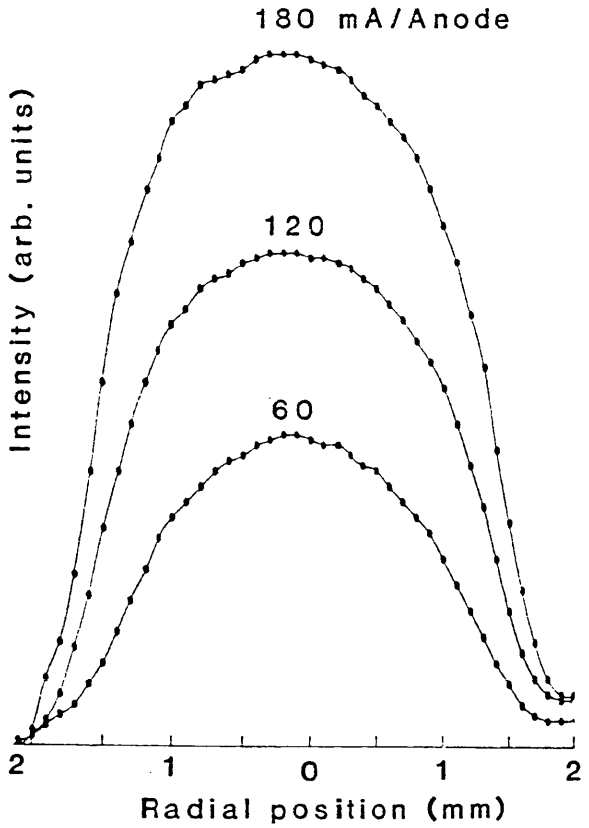

Figure 6.4 4416 Å radial intensity as a function of current.

P = 20 Torr

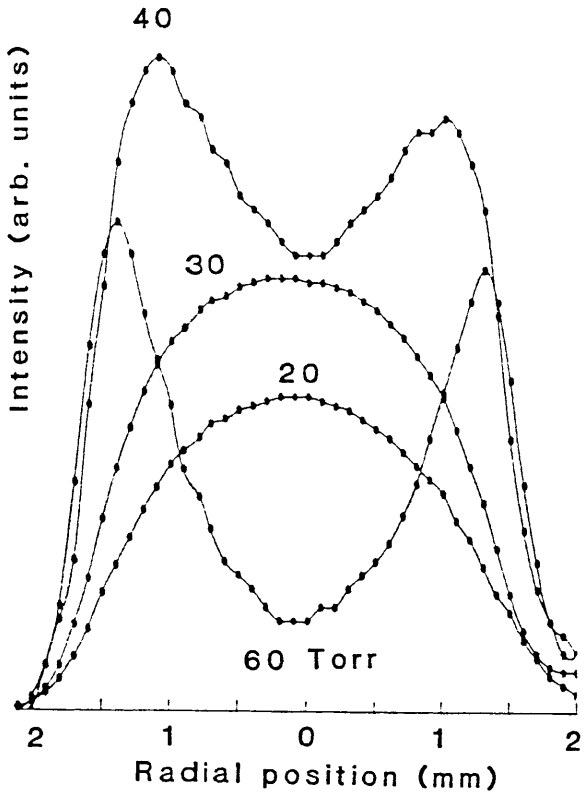

Figure 6.5 4416 Å radial intensity as a function of helium pressure.

I = 120 mA/anode

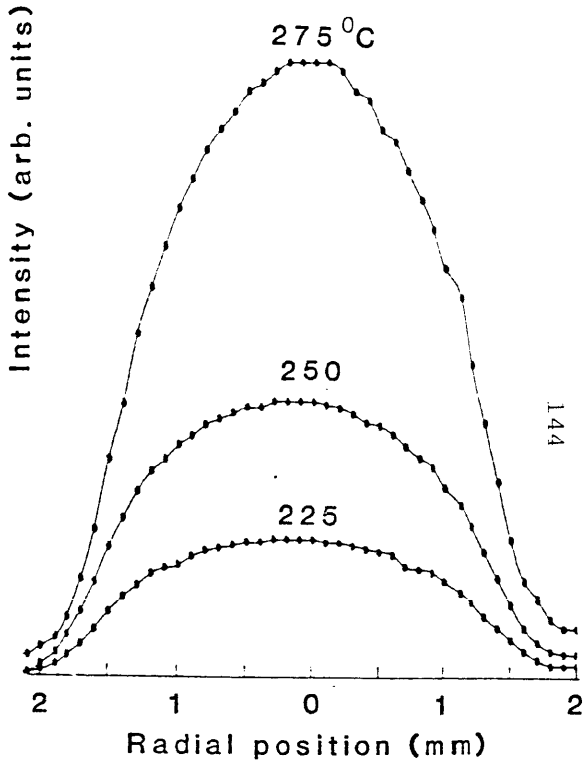

Figure 6.6 4416 Å radial intensity as a function of cadmium concentration.

P = 20 Torr

I = 120 mA/anode

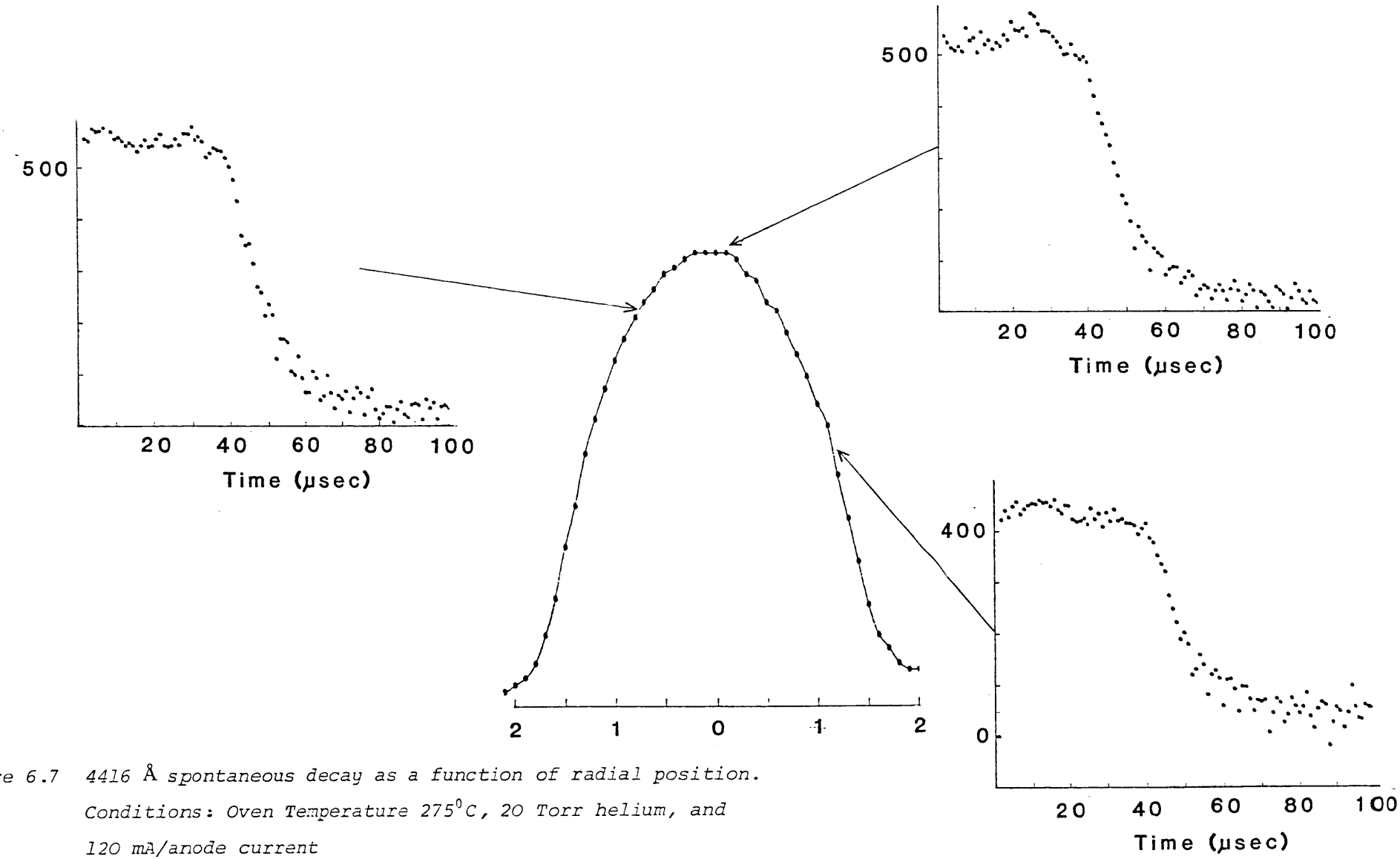

Figure 6.7 *4416 Å spontaneous decay as a function of radial position. Conditions: Oven Temperature 275°C, 20 Torr helium, and 120 mA/anode current*

6.3 SLOW ELECTRON COLLISIONS POPULATING THE $5s^2\ ^2D_{5/2}$ LEVEL OF CD II

Collisional redistribution of the excited ion densities could provide a possible mechanism explaining the early afterglow characteristics of the 4416 Å spontaneous emission. Densities of the higher lying Cd II levels, in particular, the $5s^2\ ^2D_{3/2}$ level and those excited by thermal energy charge transfer collisions are expected to be large, having values of a similar magnitude to the $5s^2\ ^2D_{5/2}$ level. This mechanism could only be investigated indirectly and, as knowledge of collision cross sections is limited, only estimates of the significance of these processes is attempted.

As the $5s^2\ ^2D_{3/2}$ level lies only $\sim$leV above the $5s^2\ ^2D_{5/2}$ level, electronic de-excitation of the former to the latter was thought to play a significant role in the early afterglow. The $5s^2\ ^2D_{3/2} \longrightarrow 5s^2\ ^2D_{5/2}$ transfer requires only a J changing electronic collision and since the interaction potential involves long range Coulomb forces, the rate coefficient for this process is expected to be large, of the order 10^{-6} cm^3 s^{-1} (Green and Webb, 1975). As the initial electron density is large (10^{13} cm^{-3}) then this result suggests that the $J = 3/2 \longrightarrow J = 5/2$ transfer could occur in times of the order of 100 nsec which is comparable with the 300 nsec radiative lifetime of the $5s^2\ ^2D_{3/2}$ level.

To evaluate the efficiency of this process an attempt was made to measure the decay of the 3250 Å ($5s^2\ ^2D_{3/2} - 5p\ ^2P_{1/2}$) transition of Cd II. If this transition showed the same characteristics as the 4416 Å decay then both have a common origin but if, on the other hand, the 3250 Å transition shows a rapid decrease in the early afterglow then

conversion of the $J = 3/2 \longrightarrow J = 5/2$ level must at least partially explain the experimental observations.

Attempts were made to measure the decay of the 3250 Å transition using the experimental apparatus described in section 4.2. However, the existing experimental difficulties (discussed in sections 4.3 and 5.2.3) were compounded by the low efficiency of the photomultiplier tube in this region of the spectrum. To improve the quality of the data, yet maintaining a fast response of the recording and detection systems, attempts were made to record data at high oven temperatures and discharge currents and with long ($\sim$20 min) data accumulation periods. Also, some relaxation of the spectrometer bandpass was required but this option was limited because of the close proximity of the strong Cd I 3261 Å intercombination transition.

In view of the poor quality of the data the results of this investigation were not convincing. The 3250 Å decay showed characteristics similar to that of the 4416 Å decay indicating that the transfer of the $5s^2\ ^2D_{3/2}$ level to the $5s^2\ ^2D_{5/2}$ level is not a significant process in the early afterglow. Further evidence supporting this conclusion was inferred from the current dependence of the early afterglow 4416 Å decay. As the rate coefficient for the $J = 3/2 \longrightarrow J = 5/2$ transfer is almost independent of electron temperature (Green and Webb, 1975) then, to a first approximation, the rate at which the process proceeds must be proportional to the electron density, which increases with discharge current. As the population density of the $5s^2\ ^2D_{3/2}$ level is expected to be of the same magnitude as the $5s^2\ ^2D_{5/2}$ level, and both have the same origin, we would expect the $5s^2\ ^2D_{5/2}$ density increase through $J = 3/2 \longrightarrow J = 5/2$ transfer to be proportional

to current. In fact the opposite is observed and thus we are forced to conclude that electronic relaxation of the $5s^2\ ^2D_{3/2}$ level to the $5s^2\ ^2D_{5/2}$ level does not produce a significant change in the population of the latter.

As the densities of the higher lying Cd II levels ($n \geq 6$) may also be expected to be large as they are populated by Penning collisions or thermal energy charge transfer collision processes, collisional redistribution of these levels also offers a mechanism by which the $5s^2\ ^2D_{5/2}$ level increases in the afterglow. Indeed these processes have previously been assumed to be occurring amongst the higher lying levels of Cd II (Webb, private communication). No collision cross section data are available for these processes but the inverse current dependence of the relative peak height would suggest that the mechanism is also an unlikely candidate to explain the intensity increase of the 4416 Å decay.

6.4 RECOMBINATION OF Cd^{++}

The close proximity of the Cd^{++} ground state to that of neutral cadmium, coupled with the existence of a large number of high energy electrons in the hollow cathode discharge, suggest that doubly ionized cadmium might be a significant ionic species in the steady state discharge. In view of the fact that the early afterglow region of the He-Cd^+ discharge has a large proportion of thermalized electrons, recombination of Cd^{++} and the subsequent decay to the $5s^2\ ^2D_{5/2}$ level could provide an efficient means for populating this level in the afterglow.

The role of the high energy electrons in the d.c. He-Cd discharge was amply demonstrated by the observation of spectral transitions amongst

the high lying levels of the helium ion, in particular the $nf\,^2F^o_{(5/2,7/2)} \longrightarrow 3d^2\,D_{(3/2,5/2)}$ $(n > 4)$ transitions which lie approximately 30 eV above the helium ground state. Careful spectroscopic examination of the steady state discharge using a 0.5m Ebert scanning spectrometer, photomultiplier (S20 response) and phase sensitive detection did not reveal the existence of any transitions amongst the higher lying levels of Cd III. Further, since the recombination rate is proportional to $(n_e)^2$ and the ion densities increase with discharge current, the efficiency of this process should increase at least quadratically with this parameter. If this mechanism is responsible for the observed intensity variations of the 4416 Å spontaneous emission then the relative peak height should also exhibit a similar variation. As discussed in section 4.5.2 this feature is not observed and in fact the relative peak height decreases with discharge current. A similar conclusion is also reached from consideration of the pressure dependence of the 4416 Å decay.

In view of these observations, it is difficult to see how recombination of Cd^{++} offers a plausible explanation for the observed variations of the 4416 Å intensity increase in the early afterglow.

6.5 MECHANISMS WHICH MAY CAUSE CHANGES IN THE He (2^3S) POPULATION

The one remaining explanation of the early afterglow characteristics of the 4416 Å spontaneous emission is that the Penning collision mechanism alone is responsible for exciting the $5s^2\,^2D_{5/2}$ level and the intensity variations merely reflect the changes in the He (2^3S) density

in the afterglow. In this section, the processes which can directly affect the He (2^3S) density are investigated and the significance of these to the early afterglow characteristics of the 4416 Å decay assessed.

In the early afterglow of the He-Cd hollow cathode discharge the high electron densities and low electron temperatures could mean that the following processes will play important roles in changing the population of the 2^3S level.

1. Three-body recombination, i.e.

$$He^+ + e + e \rightarrow He\ (2^3S) + e \qquad (6.1)$$

leading to an increase in the metastable density in the early afterglow.

2. Slow electron collisions and/or radiative decay from higher lying helium levels leading to the formation of the triplet metastable species in the early afterglow, i.e.

$$(He)^* \xrightarrow[e]{h\nu} He\ (2^3S) \qquad (6.2)$$

3. Electron collisional de-activation of the He (2^3S) level in the early afterglow, i.e.

$$He\ (2^3S) + e_{slow} \rightarrow He\ (1^1S) + e_{fast} \qquad (6.3)$$

Each of these mechanisms will now be discussed in turn.

6.5.1 Recombination

The high helium ion and electron densities and low electron temperature in the early afterglow could result in a high probability of

helium ion-electron recombination (equation 6.1). This results from the fact that recombination is proportional to $n_e^3(T_e)^{-9/2}$ (Hinnov and Hirschberg, 1962). If recombination is occurring, then the consequences of this mechanism should be evident in the afterglow decay of the He I transitions. The decay of transitions in the series $n^3D - 2^3P$ ($n > 3$) was investigated firstly in a "pure" helium discharge and secondly in a discharge containing cadmium.

Results in "Pure" Helium

The helium discharge used in these experiments was deemed "pure" in the sense that, after thoroughly washing the tube with HCl to eliminate any cadmium, no Cd I or Cd II spectral lines were visible.

All the helium lines in the $n^3D - 2^3P$ ($n > 3$) series exhibit a temporal response identical to that shown in Figure 6.8 for the 4471 Å ($4^3D - 2^3P$) transition. The shape of the decay is characteristic of recombination, with a sharp fall in intensity as electron excitation processes decay followed by a peak due to electron cooling increasing the recombination rate and a subsequent slow decay as both the electron and ion densities decrease. Evidence supporting the claim that the phenomenon shown in Figure 6.8 is due to three-body recombination comes from a study of the pressure, current and principal quantum number dependences of the afterglow intensity.

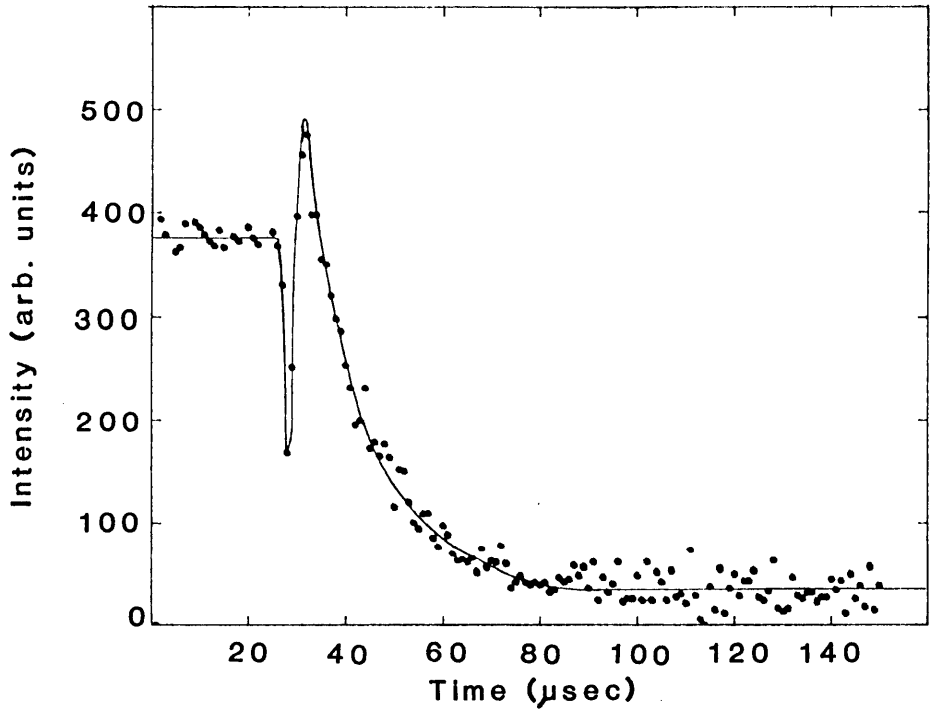

Figure 6.8 Decay of the HeI 4471 Å transition in a "pure" helium discharge for a helium pressure of 20 Torr and a discharge current of 120 mA/anode

Figures 6.9a - 6.9e show the pressure dependence of the 4471 Å decay. At low pressure (<10 Torr) the helium ion and electron densities are low and the electron temperature is high, resulting in a low rate of recombination. With increasing pressure the helium ion and electron densities increase while the electron temperature decreases and the net result is an increasing probability for recombination. Figures 6.9 also show that with increasing pressure the time to the peak of the afterglow radiation decreases, which is again consistent with the recombination model.

If recombination proceeds by the three body process represented by equation 6.1 then, as the recombination rate is proportional to $(n_e)^3$ (Hinnov and Hirschberg, 1962), the afterglow peak height should scale

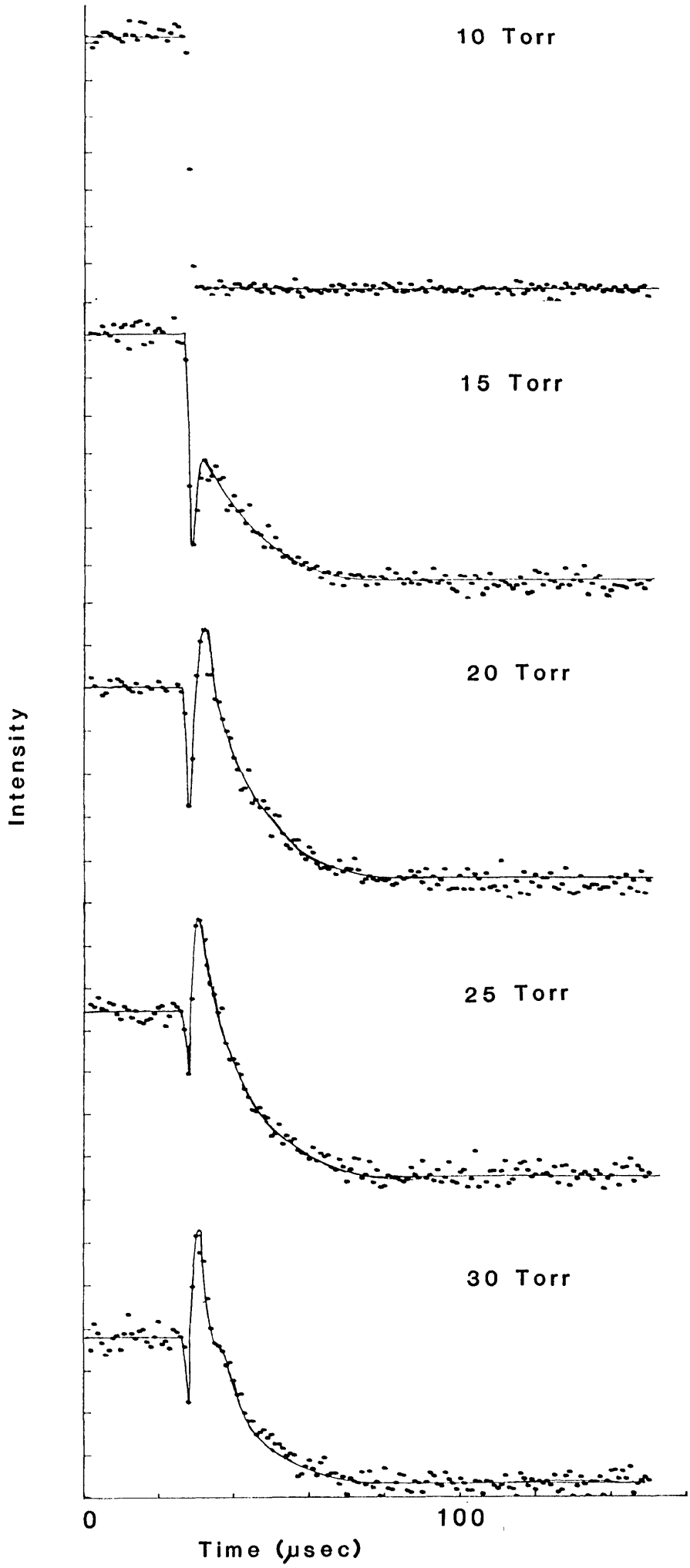

Figure 6.9a

Figure 6.9b

Figure 6.9c

Figure 6.9d

Figure 6.9e

accordingly. While it is tempting to simply state that

$$n_e \propto \text{discharge current}$$

this proportionality gives misleading results since, for these experiments involving measurement of the endlight intensity from single, isolated discharge segments, the discharge volume also varies with current (section 2.4) and thus the electron density is not proportional to current rather, it is proportional to the current density.

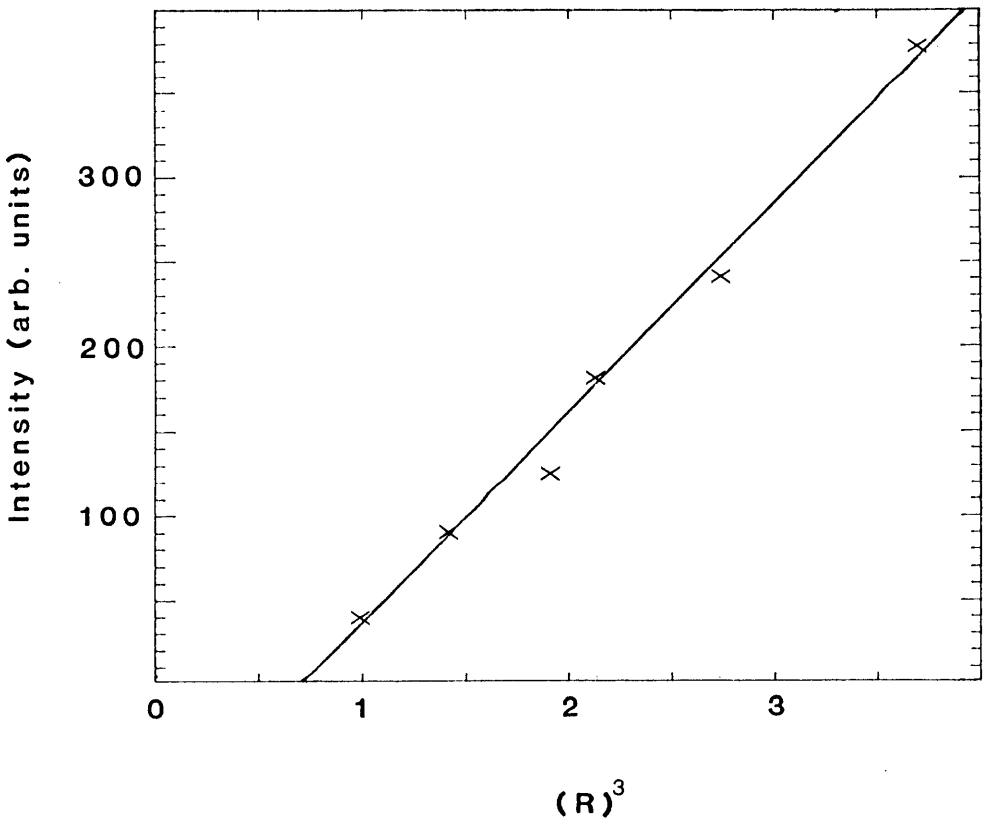

Figure 6.10 The 4471 Å afterglow peak intensity as a function of the parameter R^3 at a constant pressure of 20 Torr

Using the discharge length data of MacKellar (1978) the ratio

$$R = \frac{\text{Current density at ImA/Anode}}{\text{Current density at 60mA/Anode}}$$

was calculated. [The ratio was calculated to remove the unknown electron density from the calculations.] If the three body process is predominant in the He afterglow then the peak height should be proportional to $(R)^3$. As shown in figure 6.10 such a graph yields a straight line and thus the experimental observations are consistent with the notion that the three body recombination process is dominant in the helium afterglow.

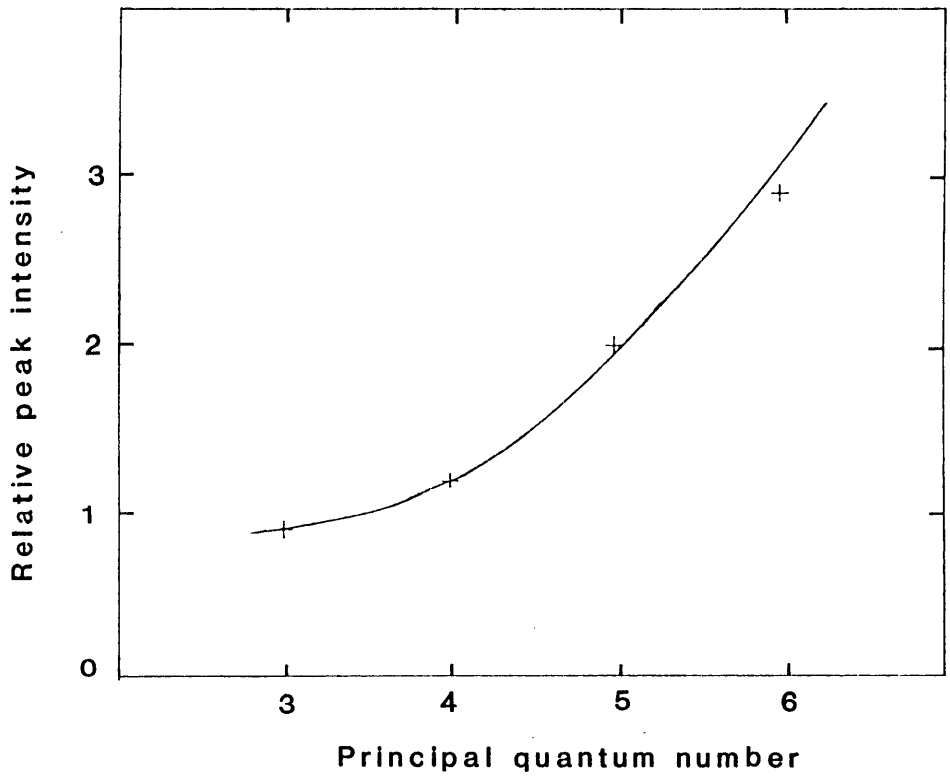

Figure 6.11 Relative peak intensity as a function of the principal quantum number for the n^3D-2^3P ($n \geq 3$) series of HeI at a constant pressure of 20 Torr and a current of 120 mA/anode

Figure 6.11 shows the relative peak intensity (afterglow intensity/steady state intensity) graphed as a function of the principal quantum number n for the $n^3D - 2^3P$ ($n > 3$) series of He I. This increase in relative peak height with increasing quantum number is easily explained in terms of three-body recombination since this process will populate more efficiently the high lying states of He I which normally have only a small steady state population.

Results in Helium-Cadmium

When cadmium is added to the discharge region a distinct change in the afterglow behaviour of the He I transitions is noted and the evidence for the existence of recombination all but disappears. Comparison of Figure 6.12 and 6.9c highlights the difference in the afterglow characteristics of the 4471 Å transition in He-Cd and "pure" helium.

At low oven temperatures ($<225^{\circ}C$) and high helium pressures ($p>35$ Torr) there was some evidence of recombination but the effect was slight and completely disappeared for higher cadmium concentrations.

This lack of visibility of the recombination radiation might be due to one of the three possible processes: (1) electron collisions redistributing the high lying helium states (He^*) more rapidly than radiative decay; (2) Penning collisions consuming He^* faster than they can radiate and; (3) charge transfer collisions destroying the helium ions more efficiently than recombination.

If electron de-excitation of the high lying levels occurs more rapidly than spontaneous decay this would lead to a reduction in the

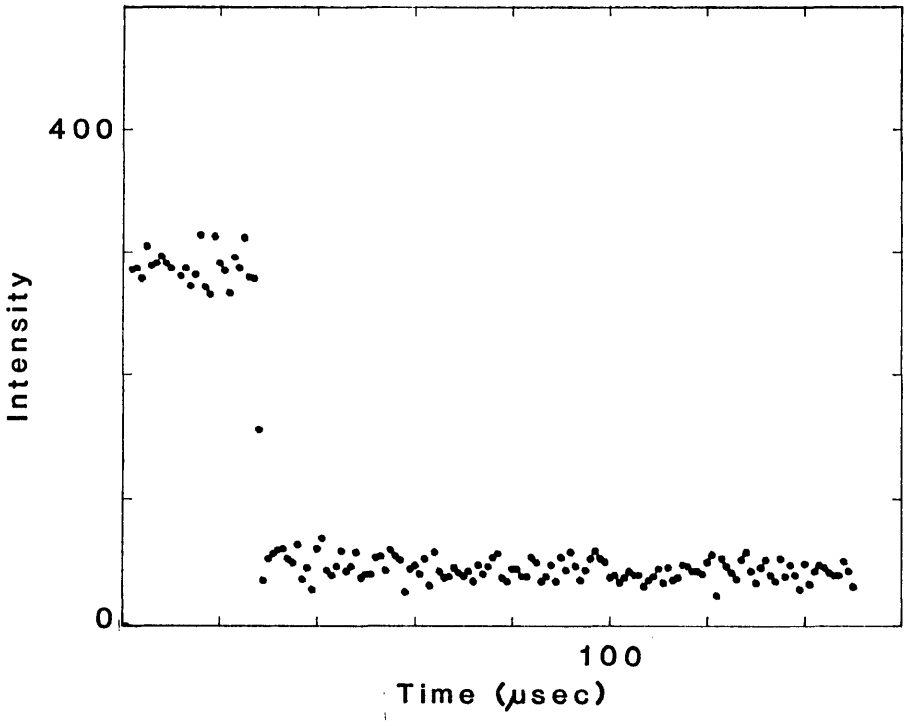

Figure 6.12 4471 Å decay when cadmium is added to the discharge volume. Conditions: 225°C Oven Temperature, 20 Torr helium, 120 mA/anode discharge current

recombination radiation. The ratio of spontaneous decay to the electron de-excitation rate is given by

$$\gamma_e = \frac{\eta A_{ul}}{n_e \langle \sigma_{de\text{-}ex} v \rangle}$$

where A_{ul} is the total spontaneous decay rate to all other levels, η the trapping coefficient to account for self absorption and $n_e\langle\sigma_{de\text{-}ex}v\rangle$ the

total electron de-excitation rate to all other levels.

For the 4^3D level (the upper level of the 4471 Å transition) the de-excitation rate was calculated from the semi-empirical cross section data of Fujimoto (1978) and an assumed Maxwellian velocity distribution for the electrons. Using this result, together with the electron density determined in Chapter 3 and the A coefficients obtained from Weise, Smith and Glennon (1966), it was found that $\gamma_e \simeq 1$ and that γ_e was only weakly dependent upon the electron temperature.

It thus appears that electron de-activation of the levels is as fast as radiative decay. However, since the only difference between the helium and helium cadmium discharge in terms of the calculation of γ_e is in the electron temperature, and γ_e is only weakly dependent on this parameter, it can be argued that electron de-activation cannot account for the difference in the shapes of the 4471 Å decay curves.

Penning collisions between helium atoms in levels other than the singlet or triplet metastable states with cadmium could provide an efficient loss mechanism for these levels and again result in an apparent loss in visibility of the recombination radiation. To investigate this, the ratio (γ_r) of the radiative to Penning decay rates was calculated from

$$\gamma_r = \frac{\eta A_{ul}}{N_{cd} < \sigma_p^u v >}$$

for a helium level u.

The Penning cross sections (σ_p^u) have only been measured for the 2^3S and 2^1S helium levels and not for other high lying states but, following Mori (1978), they may be assumed to be the same as for the helium 2^3S and

2^1S metastables. Using the Penning rate and cadmium densities calculated in Chapter 5 and assuming that $\eta=1$ in the afterglow (this will be true for all transitions except possibly those terminating on the metastable levels), the ratio γ_r was calculated. It was found that, except for oven temperatures above 275°C, $\gamma_r >> 1$ and thus Penning collisions between the non-metastable helium atoms with cadmium could not account for the change in afterglow characteristics of the He I transition.

Since Penning collisions and electron knockdown do not explain the difference in temporal response of the He I transitions in a "pure" helium and He-Cd afterglow, this suggests that the addition of cadmium to the discharge region must provide an alternative loss mechanism for the helium ions. This process must be that of thermal energy charge transfer with cadmium, i.e.

$$He^+ + Cd \rightarrow He + (Cd^+)^* \qquad (6.4)$$

Using the three-body recombination coefficient of Hinnov and Hirschberg (1962) of

$$\alpha = 5.60 \times 10^{-27} [n_e(cm^{-3})][kT_e(eV)]^{-9/2} \qquad (6.5)$$

and the thermal charge transfer cross section of Collins et al. (1971) of

$$\sigma_{TH} = 3.7 \times 10^{-15} \text{ cm}^2$$

the ratio γ_{th} of the thermal charge transfer rate to three-body recombination rate was calculated from

$$\gamma_{th} = \frac{N_{cd} < \sigma_{th} v >}{\alpha n_e}$$

and it was found that $\gamma_{th} < 1$ for low cadmium concentrations and $\gamma_{th} > 1$ for high cadmium concentrations.

Thus theory predicts that at low oven temperatures recombination dominates the helium ion loss mechanism whereas the experimental evidence would suggest otherwise. The failure of theory to predict this result could be due to a number of factors. The value of the recombination coefficient (α) could be too large or the thermal energy charge transfer cross section (σ_{th}) too small. Alternatively, because of electron heating due to de-excitation of the helium triplet metastable atoms the electron temperature in the afterglow could increase. Since the recombination coefficient varies as $T_e^{-9/2}$ any increase in electron temperature would have a dramatic effect on the value of α.

The large uncertainties associated with many of the rate coefficients used in the theoretical estimates means that this approach should be treated with caution. On the other hand the experimental results show, beyond doubt, that recombination is not occurring at a significant rate in the He-Cd afterglow. Thus, this process is not a significant population mechanism for the He (2^3S) metastable species when the discharge contains significant amounts of cadmium.

6.5.2 Electron De-excitation of the Helium 2^3S Metastable Atom

In the analysis of the data presented in Chapters 4 and 5 it was assumed that electron de-excitation of the metastable level was negligible. Although this assumption is justified late in the afterglow when the electron density has decayed, it is not necessarily so at early

times where the electron density is high (typically $\sim 10^{13}$ cm^{-3}) and the temperature low (typically <0.2eV).

The de-excitation rate is given by

$$R_{de\text{-}ex} = n_e(t) \int_{\xi_{th}}^{\infty} \left(\frac{2e}{m}\right)^{\frac{1}{2}} \sigma(\xi)\ f(\xi)\ d\xi \qquad (6.6)$$

where $\sigma(\xi)$ is the de-excitation cross section and $f(\xi)$ the electron energy distribution function. The value of the integral in equation (6.6) was evaluated from the semi-empirical cross section data of Fujimoto (1978) using detailed balancing and assuming a Maxwellian distribution for the electron velocities. The calculated collision rate, for an assumed T_e of 1000 K, is

$$R_{de\text{-}ex} \simeq n_e(t) \times 4.2 \times 10^{-9}\ \text{sec}^{-1} \qquad (6.7)$$

If the initial electron density is assumed to be $n_e = 3 \times 10^{13}$ cm^{-3} (Chapter 3, Figure 3.2) the calculated electron knockdown rate of $\sim 10^5$ sec^{-1} is of similar magnitude to the Penning collision rate (5×10^4 - 5×10^5 sec^{-1}) for the oven temperature range studied. It is clear that, in the early afterglow, super elastic collisions are a significant loss mechanism for the He (2^3S)level. The overall importance of this process can only be estimated as the electron temperature, required for the calculation of the collision rate, is not known with sufficient certainty.

6.5.3 De-excitation of Higher Lying Helium Levels into the He (2^3S) Level

From Chapter 3 the only helium levels, apart from the 2^3S state, with significant densities are 2^1S, 2^1P and 2^3P. Relaxation of these into the triplet metastable level could provide a mechanism for triplet metastable density increase in the early afterglow.

As discussed in section 5.3, the decay of the 2^1S metastable density could only be explained if singlet to triplet conversion was the dominant loss mechanism at low oven temperatures. Since the steady state singlet density is 20-30% of the triplet density and singlet to triplet conversion is a rapid process, this process provides an efficient means of populating the He (2^3S) density in the early afterglow. Phelps (1955) in studies of a pure helium afterglow has observed a 2^3S metastable density increase and attributed this phenomenon to singlet to triplet conversion.

Using the data of Fujimoto (1978) the collision cross sections for the processes

$$2^1P + e \rightarrow 2^3S + e$$

$$2^3P + e \rightarrow 2^3S + e$$

shown in Figure 6.13, are comparable to that of singlet to triplet conversion. Thus, the rate at which 2^3P and 2^1P levels are converted to the 2^3S level will be of a similar magnitude to that calculated for singlet to triplet conversion and hence electron de-excitation is expected to provide an efficient means for relaxing the high lying helium levels and thus populating the 2^3S level in the afterglow.

Also, the 2^3P level is optically connected to the 2^3S level with a lifetime of ∿40 nsec (Weise, Smith and Glennon, 1966), and therefore radiative decay of the 2^3P level will also result in the production of helium 2^3S metastable atoms.

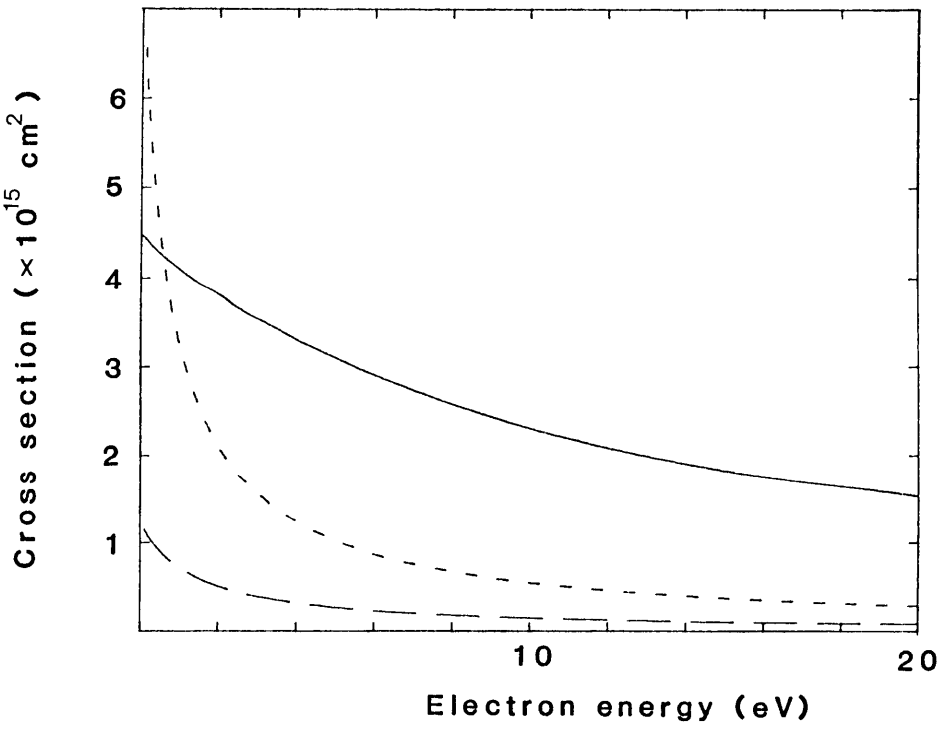

Figure 6.13 Comparison of the collision cross section data of Fujimoto for 2^3P, 2^1P and 2^1S conversion to the 2^3S level

——— $2^3P \rightarrow 2^3S$

— — $2^1P \rightarrow 2^3S$

– – – – $2^1S \rightarrow 2^3S$

6.6 DECAY OF THE GAS TEMPERATURE (T_g) IN THE AFTERGLOW

As discussed in Appendix A2 the axial gas temperature is, in general, much greater than that of the cathode wall and it might be expected that the gas temperature would decay in the afterglow. Any variation in the gas temperature would result in a time-dependent Penning collision rate and lead to the faster than linear decay (on a semi-logarithmic plot) of the 4416 Å intensity early in the afterglow. However, the temperature relaxation rate will be a diffusion dominated process and for the helium pressures used in this study is much slower than the afterglow events being investigated and thus the temperature will remain effectively constant.

This assumption is supported by the studies of a pure helium afterglow by Deloche et al. (1976) who found that for helium pressures and gas temperatures similar to those in the present discharge no variation of the gas temperature was observed during the first 2-3 msec of the afterglow.

6.7 EFFECT OF A RESIDUAL FIELD ON THE 4416 Å DECAY

The discussion of the previous sections indicates that the early afterglow behaviour of the 4416 Å spontaneous emission can be explained by variations in the metastable density due to slow electron collisions populating and depopulating this level. For reasons already discussed (Chapter 5) it is very difficult to obtain direct experimental confirmation of the changes in the 2^3S density but indirect evidence

indicating the importance of slow electron collisions in the decay scheme of the 4416 Å spontaneous emission can be obtained from the following simple experiment. If, when the discharge is pulsed, the electron temperature is maintained at a high value by the presence of a small electric field then the effects of this increased electron temperature should be evident in the 4416 Å decay. The field, which was too small to maintain a discharge, was obtained by placing a resistor ($\sim$220Ω) in series with the transistor collector and anode pin of the pulsing circuit (Figure 4.1).

Figures 6.14 - 6.15 show a comparison of the 4416 Å decay with and without the field. Clearly, in the presence of the field the size of the peak is diminished and, as the electron temperature must be higher, this reflects the importance of slow electron collisions in the early afterglow.

6.8 CONCLUSION

In this chapter mechanisms which offer plausible explanations for the 4416 Å decay in the early afterglow were investigated. These mechanisms included

- existence of non uniform Cd II ion densities in the steady state discharge
- electron collision redistribution of high lying Cd II levels to the $5s^2\ ^2D_{5/2}$ level
- recombination of Cd^{++}
- the excitation of the $5s^2\ ^2D_{5/2}$ level being due solely to Penning collisions and the 4416 Å intensity

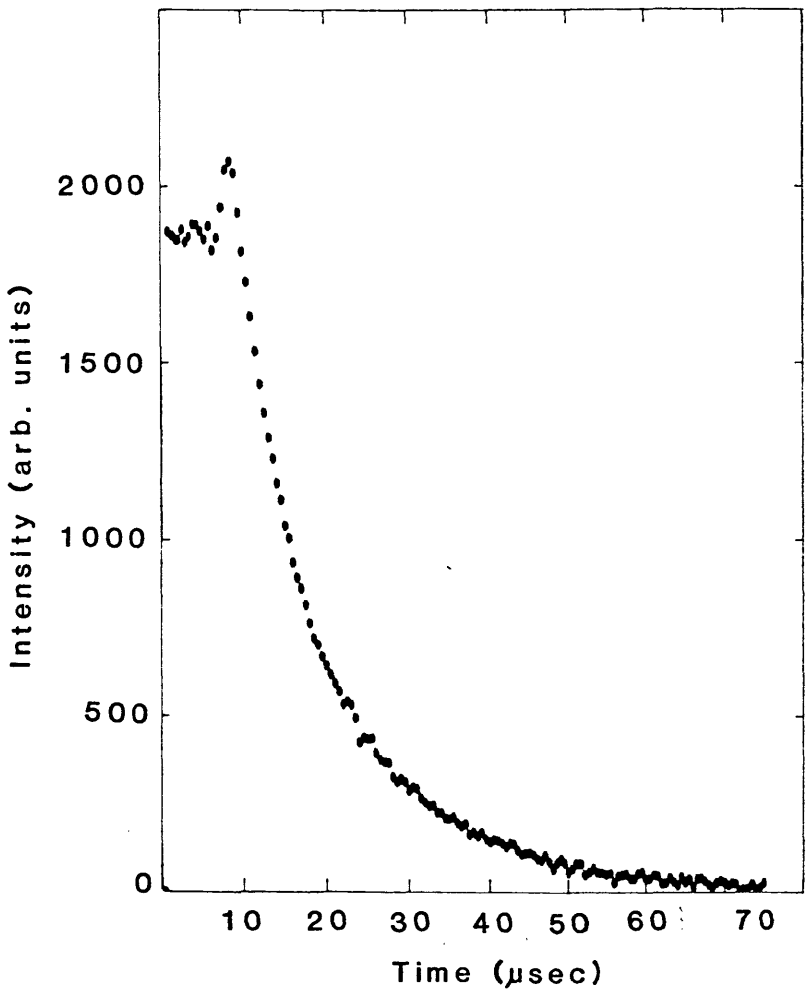

Figure 6.14 4416 Å decay under no field conditions for an oven temperature of 250°C, 20 Torr helium and 120 mA/anode discharge current

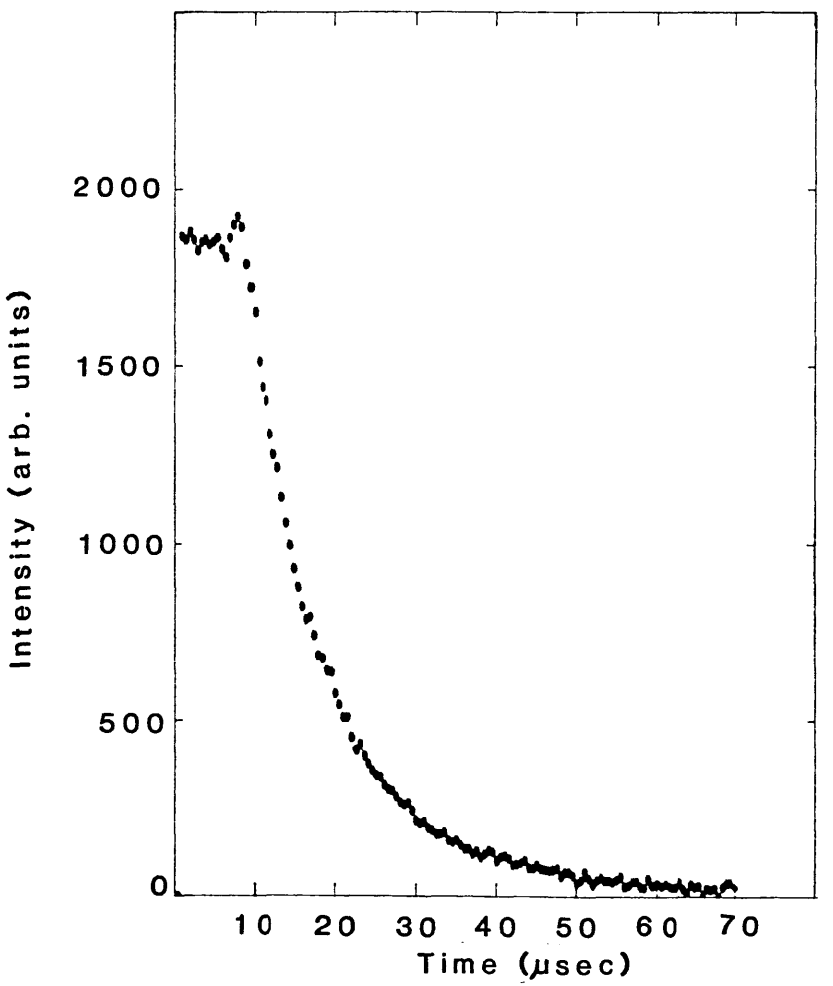

Figure 6.15 4416 Å decay when a small electric field is maintained between the anode and cathode. Conditions: as for Figure 6.14

variations reflecting the changes in the He (2^3S) density in the afterglow.

Through direct experimental verification or indirectly via interpretation of the existing data it was concluded that those mechanisms involving electronic relaxation of Cd II levels and recombination of Cd^{++} were not significant in the afterglow of the He-Cd^+ hollow cathode discharge. Similarly, it was shown that the existence of non uniform Cd II density profiles in the steady state discharge could not explain the experimental observations of the 4416 Å decay.

The only plausible explanation remaining was to assume that the Penning collision mechanism alone is responsible for populating the $5s^2\ ^2D_{5/2}$ level in the afterglow and thus the 4416 Å decay follows the temporal evolution of the He (2^3S) density in the afterglow. Processes which may affect the density of the 2^3S species were thus investigated. The processes considered were

- recombination of He^+
- electronic relaxation and/or radiative decay of higher lying He I levels
- electron de-excitation of the He (2^3S) level to the ground state.

Of these mechanisms, recombination was shown not to be a major source of 2^3S excitation in the afterglow of the He-Cd^+ discharge though it was significant in the helium afterglow. On the other hand the large initial electron densities and low electron temperatures in the early afterglow, coupled with the expected large collision cross sections for electronic relaxation of the high lying states and conversion to the ground state, meant that the rates for these processes were large, comparable with that for He (2^3S) destruction by Penning collisions.

Also, many of the higher lying triplet levels are optically connected to the 2^3S level with lifetimes against spontaneous decay of a similar magnitude as that for electronic de-excitation.

As the steady state populations of the higher lying He levels are a significant fraction of the He (2^3S) density, conversion of the former to the latter provides an efficient means of populating this level in the early afterglow. Further, in the afterglow the major loss mechanism for the 2^3S species, that of electron impact ionization, is not energetically possible this process could, in fact, increase the 2^3S density above that of its steady state value.

The role of these thermal electrons in the afterglow was demonstrated in two experimental observations. Firstly, the rapid decay of the 2^1S metastable species, reported in Section 5.4.3, was only explained if the process of $2^1S \longrightarrow 2^3S$ conversion was the dominant loss mechanism for these species in the early afterglow. Secondly, for the experiments reported the afterglow was field free but, when the 4416 Å decay was measured in the afterglow having a small field, the afterglow characteristics of the decay were substantially modified, the most noticeable change being that the magnitude of the early afterglow intensity increase was reduced.

Thus, on the basis of these observations and calculations it is proposed that the $5s^2\ ^2D_{5/2}$ level is populated solely by Penning collisions in the afterglow and that the 4416 Å intensity variations reflect those changes in the 2^3S metastable density in the afterglow. Direct confirmation of this mechanism, through measurement of the He (2^3S) decay, was not easily achieved with the experimental apparatus used in this study and thus to investigate the accuracy of the proposed

mechanism an alternative approach, that of modelling the afterglow, is attempted. The model developed for the afterglow and the results predicted by the model, form the subject of the next chapter.